LU TP 00–29
hep-ph/0007314
July 2000

Total Cross Sections and Event Properties from Real to Virtual Photons

Christer Friberg* and Torbjörn Sjöstrand*

Department of Theoretical Physics,
Lund University, Lund, Sweden

Abstract

A model for total cross sections with virtual photons is presented. In particular γ^*p and $\gamma^*\gamma^*$ cross sections are considered. Our approach extends on a model for photoproduction, where the total cross section is subdivided into three distinct event classes: direct, VMD and anomalous. With increasing photon virtuality, the latter two decrease in importance. Instead Deep Inelastic Scattering dominates, with the direct class being the $\mathcal{O}(\alpha_s)$ correction thereof. Hence, the model provides a smooth transition between the two regions. By the breakdown into different event classes, one may aim for a complete picture of all event properties.

*christer@thep.lu.se, torbjorn@thep.lu.se

1 Introduction

Traditionally, different descriptions are used for virtual and real photons. Virtual photons in the DIS (Deeply Inelastic Scattering) region are normally described as devoid of any structure, while for the real ones, the possibility of hadronic-like fluctuations play an important rôle. In the region of intermediate Q^2, it should be possible to find a description starting from either extreme. Then the language may not always be unique, i.e. a given Feynman diagram may be classified in different ways.

Several paths are possible; one is to have an explicit description in terms of higher-order Feynman diagrams [1], which then may contain several hard scales. However, in this article a main point is to obtain a smooth transition to soft physics, beyond the region of validity of perturbation theory, and then it is convenient to be able to consider transitions in one scale at a time. In the following, we will therefore develop one specific approach, where the main principle is to characterize events by a set of standard scales, such as the photon virtuality (or virtualities for $\gamma\gamma$), the photon resolution scale(s), and the hard scale of a partonic subprocess. Depending on the relative ordering of these scales, events are classified in different categories. Special emphasis is normally put on the hardest scale of the event. This may determine e.g. whether an event is classified as a DIS or a resolved photon one. Matrix elements are defined to lowest required order only, and higher-order corrections are approximated by parton showers. For instance, if the hard scale is larger than the resolution scale of the photon, a partonic evolution is allowed between the two scales. The DGLAP equations are then suitable for this evolution [2] and are to be combined with the appropriate leading-order matrix elements, responsible for the hard scattering. In a γp event, the photon resolution scale may well be smaller than both the photon virtuality and the hard-scattering scale. In this way, partly unordered evolutions in $p_\perp$ are accounted for. This is still less complete than allowed by the CCFM equations [3, 4], where the ordering may be broken in several steps, but could well provide the bulk of non-ordering effects at current energies.

The classification used here is not an economical route, however, since it leads to many event classes. For studies e.g. of the total cross section in the intermediate-Q^2 region, it is cumbersome and not necessarily better than existing approaches [5]. However, by the breakdown into distinct event classes, the road is open to provide a (more or less) complete picture of all event properties. It is this latter aspect that has then guided the model development.

As an example, the γ^*p cross section is divided into a VMD, an anomalous, a direct and a DIS component. In the limit $Q^2 \to 0$, the DIS process $\gamma^*\mathrm{q} \to \mathrm{q}$ becomes kinematically forbidden and only the first three event classes remain, reproducing the result from the photoproduction model (except for some improvements). On the contrary, when Q^2 increases from zero to high values, the resolved processes decrease in importance (as given by dipole dampening factors), the direct ones also drops (by Q^2 dependence and a shrinking phase space) and finally only the DIS process remain. At intermediate Q^2 values, the direct processes and the DIS (+parton showers) process overlap, since, in some regions of phase space, they are equally valid descriptions of the same physics. It thus becomes necessary to avoid double-counting, e.g. by introducing Sudakov style form factors for the DIS process, suppressing those parton configurations covered by the direct processes.

Based on the study of jet production by virtual photons [6] we extend the modeling to low–$p_\perp$ events. Clearly, a smooth transition from perturbative to non-perturbative physics is desired, and is achieved partly by allowing for multiple parton–parton scatterings. These

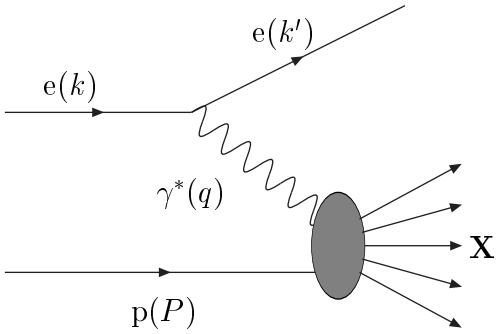

Figure 1: Deeply inelastic charged lepton-hadron scattering. (The four-momenta are given in parentheses.)

are needed to explain the underlying event activity seen in the data in hadron–hadron collisions [7], and the ideas will be taken over to the hadronic resolved photon components. At the same time, the multiple parton–parton interactions unitarize the jet cross sections, a necessity for a decent growth of the total cross section with increasing energy.

The outline of the paper is as follows. First, the different event classes are presented, including an extension to virtual photons of a model for photoproduction. How the event classes are combined, in order to avoid double-counting but still to cover the whole phase space, is described in detail. Then, results of the model are presented, with some comparisons to available data. In particular, total cross sections with virtual photons are shown with emphasis on the importance of the different event classes at various photon virtualities. Some distributions of event properties are shown to vary significantly with the photon virtuality, others less so, illustrating a complex model working smoothly between the regions of real and highly virtual photons. Similarities in γp and $\gamma\gamma$ events will be pointed out where appropriate. Finally, a summary and an outlook is given.

2 Event Classes

In the following, we begin by a reminder on the models for DIS and photoproduction, before embarking on the generalization also to intermediate virtualities in γ^*p processes. The $\gamma\gamma$, $\gamma^*\gamma$ and $\gamma^*\gamma^*$ processes thereafter follow by an application of the same rules.

2.1 Deeply Inelastic Scattering

The Deeply Inelastic Scattering of a high-energy charged lepton off a proton target, Fig. 1, involves a single electroweak boson exchange between a beam lepton and a target quark. At not too large Q^2 only photon exchange need be considered. Then the double-differential ep cross-section for DIS can be expressed in terms of the total cross-section for virtual transverse (T) and longitudinal (L) photons [8]:

$$\frac{\mathrm{d}^2\sigma(\mathrm{ep} \to \mathrm{e}\mathbf{X})}{\mathrm{d}y\,\mathrm{d}Q^2} = f^{\mathrm{T}}_{\gamma/\mathrm{e}}(y,Q^2)\sigma_{\mathrm{T}}(y,Q^2) + f^{\mathrm{L}}_{\gamma/\mathrm{e}}(y,Q^2)\sigma_{\mathrm{L}}(y,Q^2)\ , \tag{1}$$

with the fluxes

$$f^{\rm T}_{\gamma/{\rm e}}(y,Q^2) = \frac{\alpha_{\rm em}}{2\pi}\left(\frac{1+(1-y)^2}{y}\frac{1}{Q^2} - \frac{2m_{\rm e}^2 y}{Q^4}\right) , \quad (2)$$

$$f^{\rm L}_{\gamma/{\rm e}}(y,Q^2) = \frac{\alpha_{\rm em}}{2\pi}\frac{2(1-y)}{y}\frac{1}{Q^2} . \quad (3)$$

The conventional DIS variables

$$y = \frac{qP}{kP} , \quad x = \frac{Q^2}{2qP} = \frac{Q^2}{Q^2+W^2-m_{\rm p}^2} , \quad Q^2 = -q^2 , \quad W^2 = (q+P)^2 , \quad (4)$$

are related e.g. by

$$Q^2 = xy\,2kP , \quad W^2 = (1-x)y\,2kP + m_{\rm p}^2 , \quad (5)$$

where $2kP \approx (k+P)^2 = s$. Thus there are only two kinematical degrees of freedom.

The cross-sections can be related to the proton structure functions F_2 and $F_{\rm L}$ by [9, 10]

$$F_2(x,Q^2) = \frac{Q^2}{4\pi^2\alpha_{\rm em}}\frac{(1-x)Q^2}{(Q^2+4m_{\rm p}^2x^2)}(\sigma_{\rm T}+\sigma_{\rm L}) , \;\; F_{\rm L}(x,Q^2) = \frac{Q^2}{4\pi^2\alpha_{\rm em}}\frac{(1-x)Q^2}{(Q^2+4m_{\rm p}^2x^2)}\sigma_{\rm L} \quad (6)$$

and the total virtual photon-proton cross section by

$$\sigma_{\rm tot}^{\gamma^*{\rm p}} \equiv \sigma_{\rm T}+\sigma_{\rm L} = \frac{4\pi^2\alpha_{\rm em}}{Q^2}\frac{(Q^2+4m_{\rm p}^2x^2)}{(1-x)Q^2}F_2(x,Q^2) \simeq \frac{4\pi^2\alpha_{\rm em}}{Q^2(1-x)}F_2(x,Q^2) . \quad (7)$$

In the parton model,

$$F_2(x,Q^2) = \sum_{\rm q} e_{\rm q}^2 \left\{xq(x,Q^2)+x\overline{q}(x,Q^2)\right\} , \quad F_L(x,Q^2) = 0 , \quad (8)$$

to lowest order. Such an interpretation is not valid in the limit $Q^2 \to 0$, where gauge invariance requires $F_2(x,Q^2) \to 0$ so that $\sigma_{\rm tot}^{\gamma^*{\rm p}}$ remains finite. We will replace the DIS description by a photoproduction one in this limit. Hence, at small photon virtualities, the DIS process $\gamma^*{\rm q} \to {\rm q}$ should be constructed vanishingly small as compared to the contribution from the interaction of the hadronic component of the photon (to be discussed in the next section). To obtain a well-behaved DIS cross section in this limit, a $Q^4/(Q^2+m_\rho^2)^2$ factor is introduced. Here m_ρ is some non-perturbative hadronic parameter, for simplicity identified with the ρ mass. One of the $Q^2/(Q^2+m_\rho^2)$ factors is required already to give finite $\sigma_{\rm tot}^{\gamma{\rm p}}$ for conventional parton distributions, and could be viewed as a screening of the individual partons at small Q^2. The second factor is chosen to give not only a finite but actually a vanishing $\sigma_{\rm DIS}^{\gamma^*{\rm p}}$ for $Q^2 \to 0$ in order to retain the pure photoproduction description there. This latter factor thus is more a matter of convenience, and other approaches could have been pursued. Then, in the parton model, eq. (7) modifies to a DIS cross section

$$\sigma_{\rm DIS}^{\gamma^*{\rm p}} \simeq \frac{4\pi^2\alpha_{\rm em}Q^2}{(Q^2+m_\rho^2)^2}\sum_{\rm q} e_{\rm q}^2 \left\{xq(x,Q^2)+x\overline{q}(x,Q^2)\right\} . \quad (9)$$

For numerical studies, the available parton distribution parameterizations for the proton have some lower limit of applicability in both x and Q^2. For values below these minimal ones, the parton distributions are frozen at the lower limits.

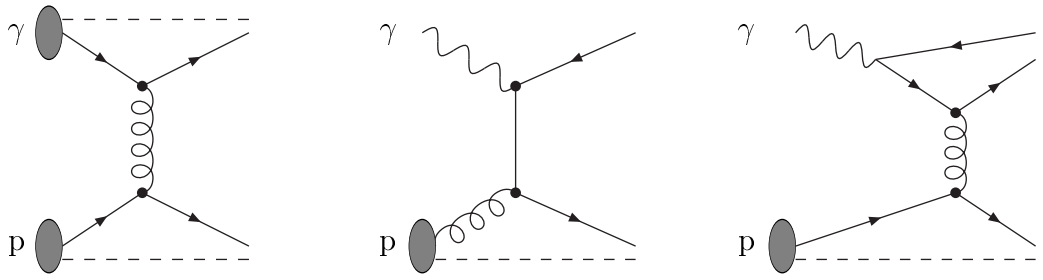

Figure 2: Contributions to hard γp interactions: a) VMD, b) direct, and c) anomalous. Only the basic graphs are illustrated; additional partonic activity is allowed in all three processes. The presence of spectator jets has been indicated by dashed lines, while full lines show partons that (may) give rise to high-$p_\perp$ jets.

2.2 Photoproduction

To first approximation, the photon is a point-like particle. However, quantum mechanically, it may fluctuate into a (charged) fermion–antifermion pair. The fluctuations $\gamma \leftrightarrow \mathrm{q\overline{q}}$ can interact strongly and therefore turn out to be responsible for the major part of the γp total cross section. The total rate of $\mathrm{q\overline{q}}$ fluctuations is not perturbatively calculable, since low-virtuality fluctuations enter a domain of non-perturbative QCD physics. It is therefore customary to split the spectrum of fluctuations into a low-virtuality and a high-virtuality part. The former part can be approximated by a sum over low-mass vector-meson states, customarily (but not necessarily) restricted to the lowest-lying vector multiplet. Phenomenologically, this Vector Meson Dominance (VMD) ansatz turns out to be very successful in describing a host of data. The high-virtuality part, on the other hand, should be in a perturbatively calculable domain.

In total, the photon wave function can then be written as

$$|\gamma\rangle = c_{\mathrm{bare}}|\gamma_{\mathrm{bare}}\rangle + \sum_{V=\rho^0,\omega,\phi,\mathrm{J}/\psi} c_V|V\rangle + \sum_{\mathrm{q=u,d,s,c,b}} c_{\mathrm{q}}|\mathrm{q\overline{q}}\rangle + \sum_{\ell=\mathrm{e},\mu,\tau} c_\ell|\ell^+\ell^-\rangle \qquad (10)$$

(neglecting the small contribution from Υ). In general, the coefficients c_i depend on the scale μ used to probe the photon. Thus $c_\ell^2 \approx (\alpha_{\mathrm{em}}/2\pi)(2/3)\ln(\mu^2/m_\ell^2)$. Introducing a cutoff parameter k_0 to separate the low- and high-virtuality parts of the $\mathrm{q\overline{q}}$ fluctuations, one similarly obtains $c_{\mathrm{q}}^2 \approx (\alpha_{\mathrm{em}}/2\pi)2e_{\mathrm{q}}^2\ln(\mu^2/k_0^2)$. The VMD part corresponds to the range of $\mathrm{q\overline{q}}$ fluctuations below k_0 and is thus μ-independent (assuming $\mu > k_0$). In conventional notation $c_V^2 = 4\pi\alpha_{\mathrm{em}}/f_V^2$, with $f_V^2/4\pi$ determined from data to be 2.20 for ρ^0, 23.6 for ω, 18.4 for ϕ and 11.5 for J/ψ [10]. The k_0 parameter is constrained by fits to F_2^γ, i.e. to the parton distributions of the photon, to be $k_0 \simeq 0.6$ GeV [11]. (The fits also contain other model uncertainties, and are only logarithmically dependent on k_0, so the precision is not high.) Finally, c_{bare} is given by unitarity: $c_{\mathrm{bare}}^2 \equiv Z_3 = 1 - \sum c_V^2 - \sum c_{\mathrm{q}}^2 - \sum c_\ell^2$. In practice, c_{bare} is always close to unity. Usually the probing scale μ is taken to be the transverse momentum of a $2 \to 2$ parton-level process.

The subdivision of the above photon wave function corresponds to the existence of three main event classes in γp events [12], cf. Fig. 2:

1. The VMD processes, where the photon turns into a vector meson before the interaction, and therefore all processes allowed in hadronic physics may occur. This includes elastic and diffractive scattering as well as low-$p_\perp$ and high-$p_\perp$ non-diffractive

events.

2. The direct processes, where a bare photon interacts with a parton from the proton.
3. The anomalous processes, where the photon perturbatively branches into a $\mathrm{q\overline{q}}$ pair, and one of these (or a daughter parton thereof) interacts with a parton from the proton.

All three processes are of $\mathcal{O}(\alpha_{\mathrm{em}})$. However, in the direct contribution the photon structure function is of $\mathcal{O}(1)$ and the hard scattering matrix elements of $\mathcal{O}(\alpha_{\mathrm{em}})$, while the opposite holds for the VMD and the anomalous processes. The $\ell^+\ell^-$ fluctuations are not interesting for us, and there is thus no class associated with them.

The difference between the three classes is reflected in the beam jet structure. The incoming proton always gives a beam jet containing the partons of the proton that did not interact. On the photon side, the direct processes do not give a beam jet at all, since all the energy of the photon is involved in the hard interaction. The VMD ones (leaving aside the elastic and diffractive subprocesses for the moment) give a beam remnant just like the proton, with a moderately small 'primordial $k_\perp$' smearing. The anomalous processes give a beam remnant produced by the $\gamma \to \mathrm{q\overline{q}}$ branching, with a transverse momentum going from k_0 upwards.

Based on the different event classes discussed above, the total photoproduction cross section can be written as

$$\sigma_{\mathrm{tot}}^{\gamma\mathrm{p}} = \sigma_{\mathrm{VMD}}^{\gamma\mathrm{p}} + \sigma_{\mathrm{direct}}^{\gamma\mathrm{p}} + \sigma_{\mathrm{anomalous}}^{\gamma\mathrm{p}} \; . \tag{11}$$

Total hadronic cross sections show a characteristic fall-off at low energies and a slow rise at higher energies. This behaviour can be parameterized by the form

$$\sigma_{\mathrm{tot}}^{AB}(s) = X^{AB} s^{\epsilon} + Y^{AB} s^{-\eta} \tag{12}$$

for $A + B \to X$. The powers ϵ and η are universal, with fit values [13]

$$\epsilon \approx 0.0808 \; , \qquad \eta \approx 0.4525 \; , \tag{13}$$

while the coefficients X^{AB} and Y^{AB} are process-dependent. Equation (12) can be interpreted within Regge theory, where the first term corresponds to pomeron exchange and gives the asymptotic rise of the cross section. The second term, the reggeon one, is mainly of interest at low energies. For the purpose of our study we do not have to rely on the Regge interpretation of eq. (12), but can merely consider it as a convenient parameterization.

The VMD part of the $\gamma\mathrm{p}$ cross section is an obvious candidate for a hadronic description. The diagonal VMD model suggests:

$$\sigma_{\mathrm{VMD}}^{\gamma\mathrm{p}}(s) = \sum_{V=\rho^0,\omega,\phi,\mathrm{J}/\psi} \frac{4\pi\alpha_{\mathrm{em}}}{f_V^2} \, \sigma_{\mathrm{tot}}^{V\mathrm{p}}(s) \; . \tag{14}$$

Assuming an additive quark model the $V\mathrm{p}$ cross sections can be parameterized as [12]

$$\begin{aligned}
\sigma_{\mathrm{tot}}^{\rho^0\mathrm{p}}(s) &\approx \sigma_{\mathrm{tot}}^{\omega\mathrm{p}}(s) \approx \frac{1}{2}\left(\sigma_{\mathrm{tot}}^{\pi^+\mathrm{p}} + \sigma_{\mathrm{tot}}^{\pi^-\mathrm{p}}\right) \approx 13.63 s^{\epsilon} + 31.79 s^{-\eta} \;\; [\mathrm{mb}] \; , \\
\sigma_{\mathrm{tot}}^{\phi\mathrm{p}}(s) &\approx \sigma_{\mathrm{tot}}^{\mathrm{K}^+\mathrm{p}} + \sigma_{\mathrm{tot}}^{\mathrm{K}^-\mathrm{p}} - \sigma_{\mathrm{tot}}^{\pi^-\mathrm{p}} \approx 10.01 s^{\epsilon} - 1.52 s^{-\eta} \;\; [\mathrm{mb}] \; , \\
\sigma_{\mathrm{tot}}^{\mathrm{J}/\psi\mathrm{p}}(s) &\approx \frac{m_\phi^2}{m_{\mathrm{J}/\psi}^2} \, \sigma_{\mathrm{tot}}^{\phi\mathrm{p}}(s) \approx \frac{1}{10} \, \sigma_{\mathrm{tot}}^{\phi\mathrm{p}}(s) \; ,
\end{aligned} \tag{15}$$

with s in GeV^2. Adding the vector meson contributions, we arrive at

$$\sigma^{\gamma \mathrm{p}}_{\mathrm{VMD}}(s) \approx 53.4 s^{\epsilon} + 115 s^{-\eta} \;\; [\mu\mathrm{b}] \; . \tag{16}$$

There is no compelling reason that such an ansatz should hold also for the total γp cross section, but empirically a parameterization according to

$$\sigma^{\gamma \mathrm{p}}_{\mathrm{tot}}(s) = X^{\gamma \mathrm{p}} s^{\epsilon} + Y^{\gamma \mathrm{p}} s^{-\eta} = 67.7 s^{\epsilon} + 129 s^{-\eta} \;\; [\mu\mathrm{b}] \tag{17}$$

does a good job [13]. For instance, these parameter values were used to predict the high-energy behaviour of the cross section, close to what was then measured by H1 and ZEUS. Thus VMD corresponds to approximately 80% of the total γp cross section at high energies, with the remaining 20% then shared among the direct and anomalous event classes.

The anomalous contribution can be written as

$$\sigma^{\gamma \mathrm{p}}_{\mathrm{anomalous}}(s) = \frac{\alpha_{\mathrm{em}}}{2\pi} \sum_{\mathrm{q}} 2 \mathrm{e}_{\mathrm{q}}^2 \int_{k_0^2}^{\infty} \frac{\mathrm{d}k_{\perp}^2}{k_{\perp}^2} \, \sigma^{\mathrm{q}\overline{\mathrm{q}}\mathrm{p}}(s; k_{\perp}) \tag{18}$$

where the prefactor and integral over $\mathrm{d}k_{\perp}^2/k_{\perp}^2$ corresponds to the probability for the photon to split into a $\mathrm{q}\overline{\mathrm{q}}$ state of transverse momenta $\pm k_{\perp}$. The cross section for this $\mathrm{q}\overline{\mathrm{q}}$ pair to scatter against the proton, $\sigma^{\mathrm{q}\overline{\mathrm{q}}\mathrm{p}}$, need to be modeled. Based only on geometrical scaling arguments (to be discussed in the next section), one could expect a decrease roughly like $1/k_{\perp}^2$. This suggests an ansatz

$$\sigma^{\mathrm{q}\overline{\mathrm{q}}\mathrm{p}}(s; k_{\perp}) = \frac{k^2_{V(\mathrm{q}\overline{\mathrm{q}})}}{k_{\perp}^2} \, \sigma^{V(\mathrm{q}\overline{\mathrm{q}})\mathrm{p}}(s) \; . \tag{19}$$

The $k_{V(\mathrm{q}\overline{\mathrm{q}})}$ is a free parameter introduced for dimensional reasons. It could be associated with the typical $k_{\perp}$ inside the vector meson V formed from a $\mathrm{q}\overline{\mathrm{q}}$ pair: $\rho^0 \approx \omega$ for u and d, ϕ for s, J/ψ for c. As a reasonable ansatz, one could guess $k_{V(\mathrm{q}\overline{\mathrm{q}})} \approx m_V/2 \approx m_{\rho}/2$. (For heavier quarks, a higher mass scale is indicated, but also a correspondingly larger lower integration limit in $k_{\perp}^2$, so the two effects cancel more or less.) Fits to the total cross section at not too high energies, with a large VMD and a small direct contributions subtracted, give corresponding numbers, $k_{V(\mathrm{q}\overline{\mathrm{q}})} \approx 0.4$ GeV for a $k_0 \approx 0.5$ GeV. These values are here related to each other: if the latter were to be changed, the former would have to be retuned accordingly. In the following we use this set of numbers. The anomalous cross section can thus be written as

$$\sigma^{\gamma \mathrm{p}}_{\mathrm{anomalous}}(s) = \frac{\alpha_{\mathrm{em}}}{2\pi} \sum_{\mathrm{q}} 2 \mathrm{e}_{\mathrm{q}}^2 \int_{k_0^2}^{\infty} \frac{\mathrm{d}k_{\perp}^2}{k_{\perp}^2} \, \frac{k^2_{V(\mathrm{q}\overline{\mathrm{q}})}}{k_{\perp}^2} \, \sigma^{V(\mathrm{q}\overline{\mathrm{q}})\mathrm{p}}(s) \tag{20}$$

To leading order, the direct events come in two kinds: QCD Compton $\gamma \mathrm{q} \to \mathrm{qg}$ (QCDC) and boson-gluon fusion $\gamma \mathrm{g} \to \mathrm{q}\overline{\mathrm{q}}$ (BGF). The cross sections are divergent in the limit $k_{\perp} \to 0$ for the outgoing parton pair. Therefore a lower cut-off is required, but no other specific model assumptions.

2.3 Combining the photoproduction processes

The VMD, direct and anomalous classes have so far been considered separately. The complete physics picture presumably would provide smooth transitions between the various

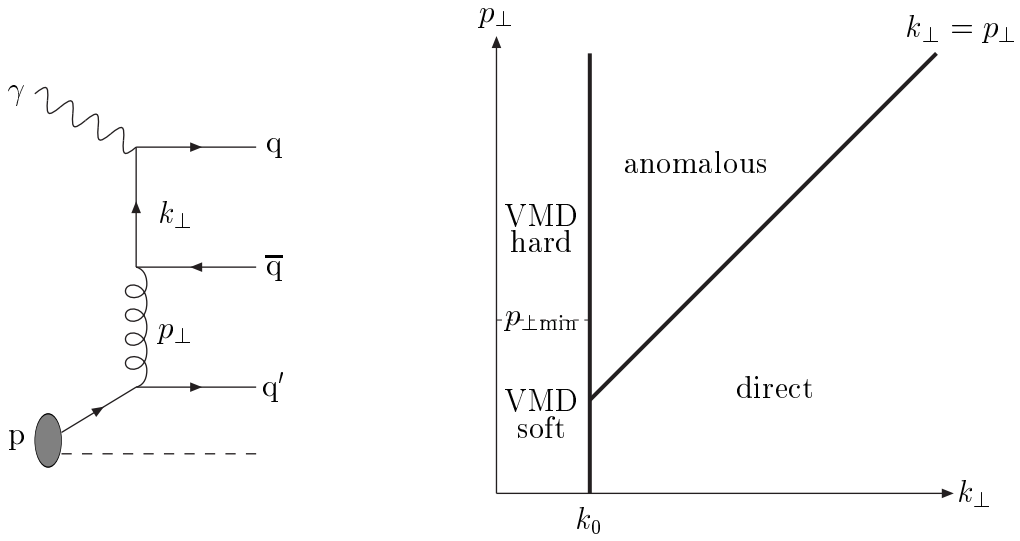

Figure 3: (a) Schematic graph for a hard γp process, illustrating the concept of two different scales. (b) The allowed phase space for this process, with one subdivision into event classes.

possibilities. To understand the relation between the processes, consider the simple graph of Fig. 3a. There two transverse momentum scales, $k_\perp$ and $p_\perp$, are introduced. Here $k_\perp$ is related to the $\gamma \to \mathrm{q}\overline{\mathrm{q}}$ vertex while $p_\perp$ is the hardest QCD $2 \to 2$ subprocess of the ladder between the photon and the proton. (Further softer partons in the ladders are omitted for clarity.) The allowed phase space can then conveniently be represented by a two-dimensional plane, Fig. 3b. The region $k_\perp < k_0$ corresponds to a small transverse momentum at the $\gamma \to \mathrm{q}\overline{\mathrm{q}}$ vertex, and thus to VMD processes. For $k_\perp > k_0$, the events are split along the diagonal $k_\perp = p_\perp$. If $k_\perp > p_\perp$, the hard $2 \to 2$ process of Fig. 3a is $\gamma\mathrm{g} \to \mathrm{q}\overline{\mathrm{q}}$, and the lower part of the graph is part of the leading log QCD evolution of the gluon distribution inside the proton. These events are direct ones. If $p_\perp > k_\perp$, on the other hand, the hard process is $\overline{\mathrm{q}}\mathrm{q}' \to \overline{\mathrm{q}}\mathrm{q}'$, and the $\gamma \to \mathrm{q}\overline{\mathrm{q}}$ vertex builds up the quark distribution inside a photon. These events are thus anomalous ones.

It should be remembered that the classification is only simple away from the border regions. When $k_\perp \approx p_\perp$, say, a description either in terms of anomalous or direct interactions would be possible. Also higher-order corrections will blur the picture, although pragmatic separations normally can be found.

A comment on the choice of variables. Instead of the squared transverse momenta $k_\perp^2$ and $p_\perp^2$ one could equally well have imagined the squared virtualities $-k^2$ and $-p^2$. However, in many processes several Feynman graphs contribute, both in the t-, u- and s-channel. The association of $p^2 = \hat{t}$ or $p^2 = \hat{u}$ is then not unique, while $p_\perp^2 = \hat{t}\hat{u}/\hat{s}$ is well-defined and coincides with $-\hat{t}$ or $-\hat{u}$ in the respective singular limit. Whether events are classified by one kind of scale or another should not be relevant, at least so long as one is consistent and stays with a leading-order description. Only for the virtual photon do we use the scale $Q^2 = -q^2 = -\hat{t}$ rather than $q_\perp^2$, in order to stay in line with conventional notation, and because there is no scale choice ambiguity here.

What complicates the picture is that an event may contain several interactions, once one considers an incoming particle as a composite object with several partons that may interact, more or less independently of each other, with partons from the other incoming

particle. Such a multiple parton–parton interaction scenario is familiar already from pp physics [7]. Here the jet cross section, above some $p_{\perp\min}$ scale of the order of 2 GeV, increases faster with energy than the total cross section. Above an energy of a few hundred GeV the calculated jet cross section is larger than the observed total one. Multiple interactions offers a solution to this apparent paradox, by squeezing a larger number of jet pairs into the average event, a process called unitarization or eikonalization. The perturbative jet cross section can then be preserved, at least down to $p_{\perp\min}$, but in the reinterpreted inclusive sense. At the same time, the unitarization plays a crucial rôle in taming the growth of the total cross section.

The composite nature of hadrons also fills another function: it regularizes the singularity of perturbative cross sections, such as $\mathrm{qg} \to \mathrm{qg}$, in the limit $p_\perp \to 0$. Perturbative calculations assume free colour charges in the initial and final states of the process, while the confinement in hadrons introduces some typical colour neutralization distance. It is the inverse of this scale that appears as some effective cutoff scale $p_{\perp\min} \simeq 2$ GeV, most likely with a slow energy dependence [14]. One possible parameterization is

$$p_{\perp\min}(s) = (1.9\ \mathrm{GeV}) \left(\frac{s}{1\ \mathrm{TeV}^2}\right)^{\epsilon} , \tag{21}$$

with the same ϵ as in eq. (13), since the rise of the total cross section with energy via Regge theory is related to the small-x behaviour of parton distributions and thus to the density of partons.

Now, if an event contains interactions at several different $p_\perp$ scales, standard practice is to classify this event by its hardest interaction. Several reasons can be given; one is that a softer interaction may be confused with QCD radiation emitted from the harder one, and thus cannot be identified on an exclusive basis. With this prescription, the cross section for an event of scale $p_\perp$ is the naive jet cross section at this $p_\perp$ scale *times* the probability that the event contained no interaction at a scale above $p_\perp$. The latter defines a form factor, related to probability conservation, analogously to but not equivalent with the Sudakov form factor of parton showers. At large $p_\perp$ values the probability of having an even larger $p_\perp$ is small, i.e. the form factor is close to unity, and the perturbative cross section is directly preserved in the event rate. At lower $p_\perp$ values, the likelihood of a larger $p_\perp$ is increased, i.e. the form factor becomes smaller than unity, and the rate of events classified by this $p_\perp$ scale falls below the perturbative answer.

We expect this picture to hold also for the VMD part of the photon, since this is clearly in the domain of hadronic physics. Thus, in the VMD domain $k_\perp < k_0$, the region of large $p_\perp$ in Fig. 3b is populated according to perturbation theory, though with nonperturbative input to the parton distributions. The region of smaller $p_\perp$ is suppressed, since the form factor here drops significantly below unity.

As one moves away from the 'pure' VMD states, such as the ρ^0, much of the same picture could well hold. Interactions at a larger $k_\perp$ value could be described in terms of some ρ' state. The uncertainty relation gives us that a state of virtuality $\simeq k_\perp$ has a maximal size $\simeq 1/k_\perp$ and thus spans an area $\propto 1/k_\perp^2$. In a naive picture, the ρ'p cross section would then drop with increasing $k_\perp$, but flatten out at a value given by the proton size. We know that this is not the scaling observed in nature, however, where e.g. the J/ψp cross section is much below the ϕp one [15]. Rather it appears that the cross section is proportional to the area of the state interacting with the proton, i.e. a (kind of) geometrical scaling. Such a behaviour becomes understandable (but not easily predicted in detail) when one remembers that the colour neutralization distance inside a

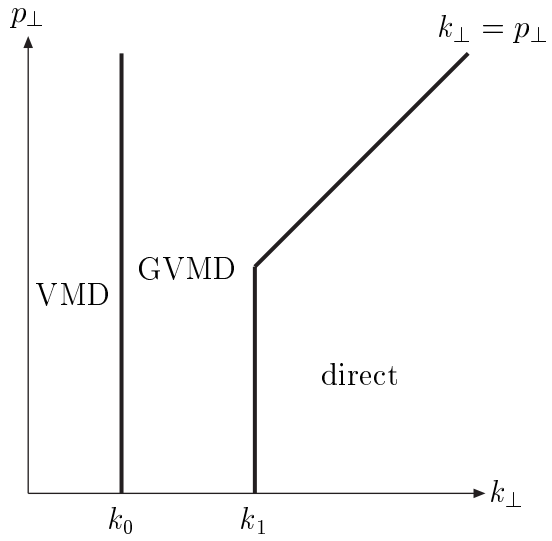

Figure 4: An alternative classification of the phase space in Fig. 3, which better takes into account unitarization effects.

more virtual photon state is also reduced, so that the interactions in general tend to be weakened by interference effects not included in the simple perturbative cross sections. This could then be the origin for a geometrical scaling like the one in eq. (19).

Alternatively to the geometric approach, the anomalous and direct cross sections for such a $k_\perp$ state could be calculated. If these latter are larger than the geometrical scaling answer, one could expect multiple interaction effects to become important and couple the two event classes. That is, the presence of an anomalous interaction of some large $p_\perp$ would preempt the event from being classifiable as a direct one with a lower $p_\perp$, in analogy with the discussion on hadronic physics above. One can even attempt eikonalized descriptions [16], although such require a number of assumptions to be made.

Calculating the perturbative anomalous cross section in the region given by $p_\perp > \max(k_\perp, p_{\perp\min}(s))$, the geometric scaling answer is exceeded for some region $k_\perp \lesssim k_1$, with $k_1 \approx 2 - 4$ GeV (higher for higher energies). Only for $k_\perp > k_1$ is the jet cross section dropping below the geometric scaling one. At these larger $k_\perp$ values, the direct rate dominates over the anomalous. As a convenient but rather arbitrary choice, for subsequent studies we put $k_1 = p_{\perp\min}(s)$, with the latter given by eq. (21). This value lies below the crossover point noted above, but the simple modified geometrical scaling picture is not precise enough that it can be trusted too far, so a separate k_1 parameterization would seem excessive.

The final scenario is illustrated in Fig. 4. The bulk of the cross section, in the region $k_\perp < k_1$, is now described by the photon interacting as dense, hadronic states, VMD for $k_\perp \lesssim k_0$ and Generalized VMD (GVMD) for $k_0 \lesssim k_\perp \lesssim k_1$. The total VMD cross section is given by the pomeron-type ansatz, while the jet cross section can be obtained from the parton distributions of the respective vector meson state. Correspondingly, the GVMD states have a total cross section based on Pomeron considerations and a jet cross section now based on the anomalous part of the parton distributions of the photon. In principle, an eikonalization should be performed for each GVMD state separately, but in practice that would be overkill. Instead the whole region is represented by one single state per quark flavour, with a jet production given by the full anomalous part of the photon

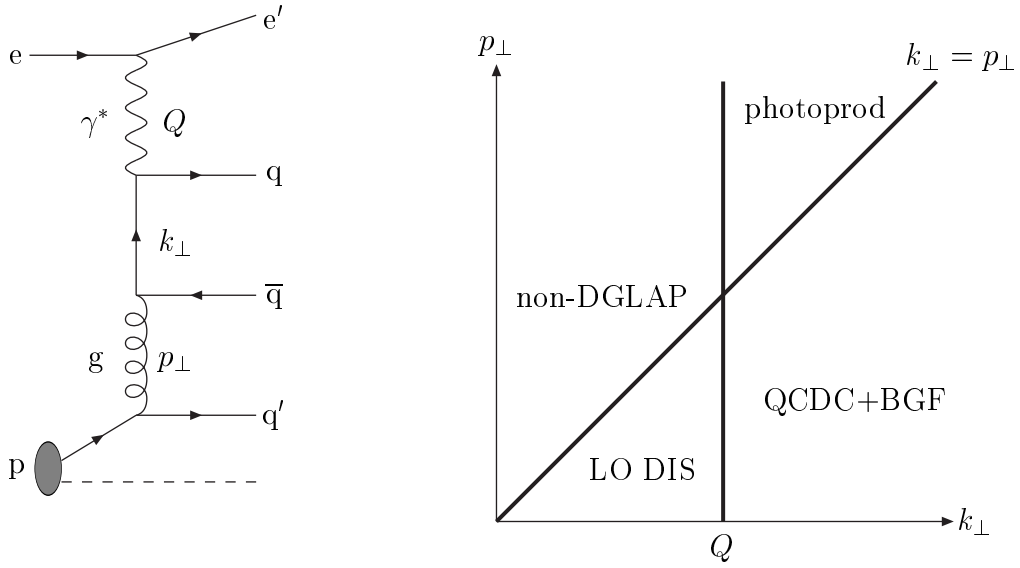

Figure 5: (a) Schematic graph for a hard γ^*p process, illustrating the concept of three different scales. (b) Event classification in the large-Q^2 limit.

distributions. By extending this jet rate also to the region $k_\perp > k_1$, one does introduce a small mismatch between the low-$p_\perp$ and high-$p_\perp$ descriptions, but retains the correct full jet rate at high $p_\perp$'s. Implicitly, the presence of a spectrum of $k_\perp$ states can be taken into account by the choice of a realistic $p_\perp$ spectrum of the photon beam remnant, maybe still without the full correlation structure between the high-$p_\perp$ and low-$p_\perp$ parts of the individual events.

Thus, post facto, the approximate validity of a Regge theory ansatz for $\sigma_{\rm tot}^{\gamma \rm p}$ is making sense. Above k_1 only the direct cross section need be considered, since here the anomalous one is negligibly small, at least in terms of total cross sections. (As noted above, we have actually chosen to lump it with the other GVMD contributions, so as not to lose the jet rate itself.) Numerically, the recipe of extending the anomalous contribution to infinity according to a GVMD scaling recipe, as is done in eq. (20), is about equally good. The latter may involve some double-counting with the direct cross section, but not more than falls within the general uncertainty of the geometric scaling and eikonalization game.

2.4 DIS revisited

In DIS, the photon virtuality Q^2 introduces a further scale to the process, i.e. one goes from Fig. 3a to Fig. 5a. The traditional DIS region is the strongly ordered one, $Q^2 \gg k_\perp^2 \gg p_\perp^2$, where DGLAP-style evolution [2] is responsible for the event structure. As above, ideology wants strong ordering, while real life normally is based on ordinary ordering $Q^2 > k_\perp^2 > p_\perp^2$. Then the parton-model description of $F_2(x, Q^2)$ in eq. (8) is a very good first approximation. The problems come when the ordering is no longer well-defined, i.e. either when the process contains several large scales or when $Q^2 \to 0$. In these regions, an $F_2(x, Q^2)$ may still be defined by eq. (7), but its physics interpretation is not obvious.

Let us first consider a large Q^2, where a possible classification is illustrated in Fig. 5b. The regions $Q^2 > p_\perp^2 > k_\perp^2$ and $p_\perp^2 > Q^2 > k_\perp^2$ correspond to non-ordered emissions,

that then go beyond DGLAP validity and instead have to be described by the BFKL [17] or CCFM [3] equations, see e.g. [4]. Normally one expects such cross sections to be small at large Q^2. The (sparsely populated) region $p_\perp^2 > k_\perp^2 > Q^2$ can be viewed as the interactions of a resolved (anomalous) photon.

The region $k_\perp^2 > Q^2 \gg 0$ and $k_\perp^2 > p_\perp^2$ contains the $\mathcal{O}(\alpha_s)$ corrections to the lowest-order (LO) DIS process $\gamma^*\mathrm{q} \to \mathrm{q}$, namely QCD Compton $\gamma^*\mathrm{q} \to \mathrm{qg}$ and boson-gluon fusion $\gamma^*\mathrm{g} \to \mathrm{q}\overline{\mathrm{q}}$. These are nothing but the direct processes $\gamma\mathrm{q} \to \mathrm{qg}$ and $\gamma\mathrm{g} \to \mathrm{q}\overline{\mathrm{q}}$ extended to virtual photons. The borderline $k_\perp^2 > Q^2$ is here arbitrary — also processes with $k_\perp^2 < Q^2$ could be described in this language. In the parton model, this whole class of events are implicitly included in F_2, and are related to the logarithmic scaling violations of the parton distributions. The main advantage of a separation at $k_\perp = Q$ thus comes from the matching to photoproduction. Also the exclusive modeling of events, with the attaching of parton showers of scale Q^2 to DIS events, is then fairly natural.

The DIS cross section thus is subdivided into

$$\sigma_{\mathrm{tot}}^{\gamma^*\mathrm{p}} \simeq \frac{4\pi^2\alpha_{\mathrm{em}}Q^2}{(Q^2+m_\rho^2)^2}F_2(x,Q^2) = \sigma_{F_2}^{\gamma^*\mathrm{p}} \simeq \sigma_{\mathrm{DIS}}^{\gamma^*\mathrm{p}} = \sigma_{\mathrm{LO\,DIS}}^{\gamma^*\mathrm{p}} + \sigma_{\mathrm{QCDC}}^{\gamma^*\mathrm{p}} + \sigma_{\mathrm{BGF}}^{\gamma^*\mathrm{p}} \; . \tag{22}$$

The $\sigma_{\mathrm{DIS}}^{\gamma^*\mathrm{p}}$ is given by eq. (9), while the last two terms are well-defined by an integration of the respective matrix element [6]. When extended to small Q^2, these two terms will increase in importance, and one may eventually encounter a $\sigma_{\mathrm{LO\,DIS}}^{\gamma^*\mathrm{p}} < 0$, if calculated by a subtraction of the QCDC and BGF terms from the total DIS cross section. However, here we expect the correct answer not to be a negative number but an exponentially suppressed one, by a Sudakov form factor. This modifies the cross section:

$$\sigma_{\mathrm{LO\,DIS}}^{\gamma^*\mathrm{p}} = \sigma_{\mathrm{DIS}}^{\gamma^*\mathrm{p}} - \sigma_{\mathrm{QCDC}}^{\gamma^*\mathrm{p}} - \sigma_{\mathrm{BGF}}^{\gamma^*\mathrm{p}} \quad \longrightarrow \quad \sigma_{\mathrm{DIS}}^{\gamma^*\mathrm{p}} \, \exp\left(-\frac{\sigma_{\mathrm{QCDC}}^{\gamma^*\mathrm{p}} + \sigma_{\mathrm{BGF}}^{\gamma^*\mathrm{p}}}{\sigma_{\mathrm{DIS}}^{\gamma^*\mathrm{p}}} \right) \; . \tag{23}$$

Since we here are in a region where $\sigma_{\mathrm{DIS}}^{\gamma^*\mathrm{p}} \ll \sigma_{F_2}^{\gamma^*\mathrm{p}}$, i.e. where the DIS cross section is no longer the dominant one, this change of the total DIS cross section is not essential. Even more, for $Q^2 \to 0$ we know that the direct processes should survive whereas the lowest-order DIS one has to vanish. Since eq. (9) ensures that $\sigma_{\mathrm{DIS}}^{\gamma^*\mathrm{p}} \to 0$ in this limit, it also follows that $\sigma_{\mathrm{LO\,DIS}}^{\gamma^*\mathrm{p}}$ does so.

2.5 From Real to Virtual Photons

It is now time to try to combine the different aspects of the photon, to provide an answer that smoothly interpolates between the photoproduction and DIS descriptions, in a physically sensible way.

A virtual photon has a reduced probability to fluctuate into a vector meson state, and this state has a reduced interaction probability. This can be modeled with the traditional dipole factors [18]

$$\sigma_{\mathrm{VMD}}^{\gamma^*\mathrm{p}}(s,Q^2) = \sum_{V=\rho^0,\omega,\phi,\mathrm{J}/\psi} \frac{4\pi\alpha_{\mathrm{em}}}{f_V^2} \left(\frac{m_V^2}{m_V^2+Q^2} \right)^2 \sigma_{\mathrm{tot}}^{V\mathrm{p}}(s) \; . \tag{24}$$

Similarly, the GVMD states are affected,

$$\sigma_{\mathrm{GVMD}}^{\gamma^*\mathrm{p}}(s,Q^2) = \frac{\alpha_{\mathrm{em}}}{2\pi} \sum_{\mathrm{q}} 2\mathrm{e}_{\mathrm{q}}^2 \int_{k_0^2}^{k_1^2} \frac{\mathrm{d}k_\perp^2}{k_\perp^2} \left(\frac{4k_\perp^2}{4k_\perp^2+Q^2} \right)^2 \frac{k_{V(\mathrm{q}\overline{\mathrm{q}})}^2}{k_\perp^2} \, \sigma^{V(\mathrm{q}\overline{\mathrm{q}})\mathrm{p}}(s) \; , \tag{25}$$

where a relation $2k_\perp \simeq m$ is assumed.

The above generalization to virtual photons does not address the issue of longitudinal photons. Their interactions vanish in the limit $Q^2 \to 0$, but can well give a non-negligible contribution at finite Q^2 [19]. A common approach is to attribute the longitudinal cross section with an extra factor of $r_V = a_V Q^2/m_V^2$ relative to the transverse one [20], where a_V is some unknown parameter to be determined from data. Such an ansatz only appears reasonable for moderately small Q^2, however, so following the lines of our previous study of jet production by virtual photons [6], we will try the two alternatives

$$r_1(m_V^2, Q^2) = a \frac{4m_V^2 Q^2}{(m_V^2 + Q^2)^2} \; , \tag{26}$$

$$r_2(m_V^2, Q^2) = a \frac{4Q^2}{(m_V^2 + Q^2)} \; . \tag{27}$$

While r_1 vanishes for high Q^2, r_2 approaches the constant value a. The above VMD expressions are again extended to GVMD by the identification $m_V \approx 2k_\perp$. The cross sections can then be written as

$$\begin{aligned} \sigma^{\gamma^*\mathrm{p}}_{\mathrm{VMD}}(W^2, Q^2) &= \sum_{V=\rho^0,\omega,\phi,\mathrm{J}/\psi} \frac{4\pi\alpha_{\mathrm{em}}}{f_V^2} \left[1 + r_i(m_V^2, Q^2)\right] \times \\ &\times \left(\frac{m_V^2}{m_V^2 + Q^2}\right)^2 \sigma^{V\mathrm{p}}_{\mathrm{tot}}(W^2) \; , \end{aligned} \tag{28}$$

$$\begin{aligned} \sigma^{\gamma^*\mathrm{p}}_{\mathrm{GVMD}}(W^2, Q^2) &= \frac{\alpha_{\mathrm{em}}}{2\pi} \sum_{\mathrm{q}} 2\mathrm{e}_{\mathrm{q}}^2 \int_{k_0^2}^{k_1^2} \frac{\mathrm{d}k_\perp^2}{k_\perp^2} \left[1 + r_i(4k_\perp^2, Q^2)\right] \times \\ &\times \left(\frac{4k_\perp^2}{4k_\perp^2 + Q^2}\right)^2 \frac{k^2_{V(\mathrm{q}\overline{\mathrm{q}})}}{k_\perp^2} \sigma^{V(\mathrm{q}\overline{\mathrm{q}})\mathrm{p}}(W^2) \; . \end{aligned} \tag{29}$$

Note that we also here replaced s by the conventional DIS variable W^2; obviously both refer to the same γ^*p squared invariant mass.

The extrapolation to $Q^2 > 0$ is trivial for the direct processes, which coincide with the DIS QCDC and BGF processes. The matrix elements contain all the required Q^2 dependence, with a smooth behaviour in the $Q^2 \to 0$ limit. They are to be applied to the region $k_\perp > \max(k_1, Q)$ (and $k_\perp > p_\perp$, as usual).

Remains the LO DIS process. It is here that one could encounter an overlap and thereby double-counting with the VMD and GVMD processes. Comparing Fig. 5b with Fig. 4, one may note that the region $p_\perp > k_\perp$ involves no problems, since we have made no attempt at a non-DGLAP DIS description but cover this region entirely by the VMD/GVMD descriptions. Also, if $Q > k_1$, then the region $k_1 < k_\perp < Q$ (and $k_\perp > p_\perp$) is covered by the DIS process only. So it is in the corner $k_\perp < k_1$ that the overlap can occur. If Q^2 is very small, the exponential factor in eq. (23) makes the DIS contribution too small to worry about. Correspondingly, if Q^2 is very big, the VMD/GVMD contributions are too small to worry about. Furthermore, a large Q^2 implies a Sudakov factor suppression of a small $k_\perp$ in the DIS description. If W^2 is large, the multiple-interaction discussions above are relevant for the VMD/GVMD states: the likelihood of an interaction at large $p_\perp$ will preempt the population of the low-$p_\perp$ region.

In summary, it is only in the region of intermediate Q^2 and rather small W^2 that we have reason to worry about a significant double-counting. As we shall see, it is indeed in

this region that the VMD/GVMD contribution does not appear to dampen quite as fast as data indicates. Typically, this is the region where $x \approx Q^2/(Q^2+W^2)$ is not close to zero, and where F_2 is dominated by the valence-quark contribution. The latter behaves roughly $\propto (1-x)^n$, with an n of the order of 3 or 4. Therefore we will introduce a corresponding damping factor to the VMD/GVMD terms. The real damping might be somewhat different but, since small W values are not our prime interest, we rest content with this approximate form.

In total, we have now arrived at our ansatz for all Q^2

$$\begin{aligned}\sigma_{\mathrm{tot}}^{\gamma^*\mathrm{p}} &= \sigma_{\mathrm{DIS}}^{\gamma^*\mathrm{p}} \exp\left(-\frac{\sigma_{\mathrm{QCDC}}^{\gamma^*\mathrm{p}}+\sigma_{\mathrm{BGF}}^{\gamma^*\mathrm{p}}}{\sigma_{\mathrm{DIS}}^{\gamma^*\mathrm{p}}}\right) + \sigma_{\mathrm{QCDC}}^{\gamma^*\mathrm{p}} + \sigma_{\mathrm{BGF}}^{\gamma^*\mathrm{p}} \\ &+ \left(\frac{W^2}{Q^2+W^2}\right)^n \left(\sigma_{\mathrm{VMD}}^{\gamma^*\mathrm{p}} + \sigma_{\mathrm{GVMD}}^{\gamma^*\mathrm{p}}\right) , \end{aligned} \tag{30}$$

where the DIS, VMD and GVMD terms are given by eqs. (9), (28) and (29), respectively, and the QCDC and BGF terms by direct integration of the respective matrix elements for the region $k_\perp > \max(k_1, Q)$. To keep the terminology reasonably compact, also for the $\gamma^*\gamma^*$ case below, we will use res as shorthand for the resolved VMD plus GVMD contributions and dir as shorthand for the QCDC and BGF processes. Then eq. (30) simplifies to

$$\sigma_{\mathrm{tot}}^{\gamma^*\mathrm{p}} = \sigma_{\mathrm{DIS}}^{\gamma^*\mathrm{p}} \exp\left(-\frac{\sigma_{\mathrm{dir}}^{\gamma^*\mathrm{p}}}{\sigma_{\mathrm{DIS}}^{\gamma^*\mathrm{p}}}\right) + \sigma_{\mathrm{dir}}^{\gamma^*\mathrm{p}} + \left(\frac{W^2}{Q^2+W^2}\right)^n \sigma_{\mathrm{res}}^{\gamma^*\mathrm{p}} . \tag{31}$$

2.6 Photon–photon collisions

A generalization of the γp picture to $\gamma\gamma$ events is obtained by noting that each of the two incoming photons is described by a wave function of the type given in eq. (10). In total, there are therefore three times three event classes. By symmetry, the 'off-diagonal' combinations appear pairwise, so for real photons the number of distinct classes is only six. These are, cf. Fig. 6:

1. VMD×VMD: both photons turn into hadrons, and the processes are therefore the same as allowed in hadron–hadron collisions.
2. VMD×direct: a bare photon interacts with the partons of the VMD photon.
3. VMD×anomalous: the anomalous photon perturbatively branches into a $\mathrm{q\overline{q}}$ pair, and one of these (or a daughter parton thereof) interacts with a parton from the VMD photon.
4. Direct×direct: the two photons directly give a quark pair, $\gamma\gamma \to \mathrm{q\overline{q}}$. Also lepton pair production is allowed, $\gamma\gamma \to \ell^+\ell^-$, but will not be considered by us.
5. Direct×anomalous: the anomalous photon perturbatively branches into a $\mathrm{q\overline{q}}$ pair, and one of these (or a daughter parton thereof) directly interacts with the other photon.
6. Anomalous×anomalous: both photons perturbatively branch into $\mathrm{q\overline{q}}$ pairs, and subsequently one parton from each photon undergoes a hard interaction.

Most of the above classes above are pretty much the same as allowed in γp events, since the interactions of a VMD or anomalous photon and those of a proton are about the same. Only the direct×direct class offer a new hard subprocess.

The main parton-level processes that occur in the above classes are:

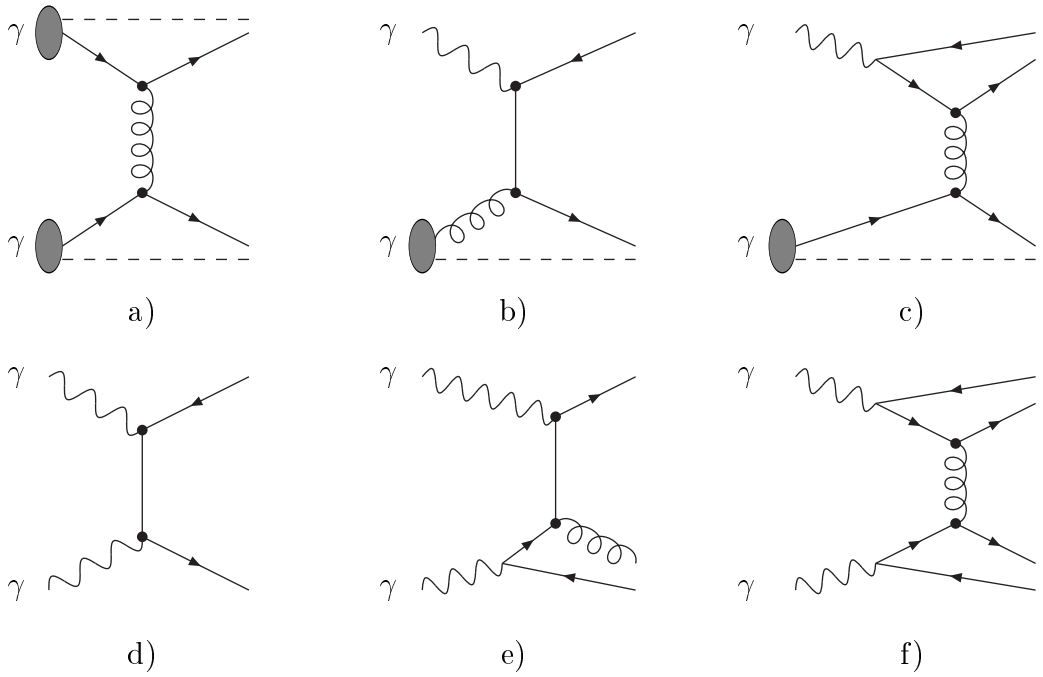

Figure 6: Contributions to hard real $\gamma\gamma$ interactions: a) VMD×VMD, b) VMD×direct, c) VMD×anomalous, d) direct×direct, e) direct×anomalous, and f) anomalous×anomalous. Notation as in Fig. 2.

- The 'direct' processes $\gamma\gamma \to \mathrm{q\overline{q}}$ only occur in class 4.
- The 'single-resolved' processes $\gamma\mathrm{q} \to \mathrm{qg}$ and $\gamma\mathrm{g} \to \mathrm{q\overline{q}}$ occur in classes 2 and 5.
- The 'double-resolved' processes $\mathrm{qq}' \to \mathrm{qq}'$ (where q' may also represent an anti-quark), $\mathrm{q\overline{q}} \to \mathrm{q}'\overline{\mathrm{q}}'$, $\mathrm{q\overline{q}} \to \mathrm{gg}$, $\mathrm{qg} \to \mathrm{qg}$, $\mathrm{gg} \to \mathrm{q\overline{q}}$ and $\mathrm{gg} \to \mathrm{gg}$ occur in classes 1, 3 and 6.

The classification of a generic Feynman diagram by the different possible components is illustrated in Fig. 7. The appearance of more scales makes it infeasible to draw diagrams like Fig. 3b, but the principles are the same.

Also the extension to virtual photons follows from the γ^*p formalism above, but now with (up to) five scales to keep track of: $p_\perp$, $k_{\perp 1}$, $k_{\perp 2}$, Q_1 and Q_2. First consider the three by three classes present already for real photons, which remain nine distinct ones for $Q_1^2 \neq Q_2^2$. Each VMD or GVMD state is associated with its dipole damping factor and its correction factor for the longitudinal contribution. The QCDC and BGF matrix elements involving one direct photon on a VMD or a GVMD state explicitly contain the dependence on the direct photon virtuality, separately given for the transverse and the longitudinal contributions. Also the direct×direct matrix elements are known for the four

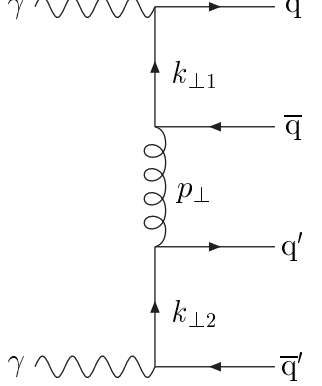

1. VMD×VMD: $k_{\perp 1}, k_{\perp 2} < k_0$, arbitrary $p_\perp$
2. VMD×direct: $k_{\perp 1} < k_0 < p_\perp < k_{\perp 2}$ + $(1 \leftrightarrow 2)$
3. VMD×anomalous: $k_{\perp 1} < k_0 < k_{\perp 2} < p_\perp$ + $(1 \leftrightarrow 2)$
4. Direct×direct: $k_0 < k_{\perp 1} = k_{\perp 2}$
5. Direct×anomalous: $k_0 < k_{\perp 1} < p_\perp < k_{\perp 2}$ + $(1 \leftrightarrow 2)$
6. Anomalous×anomalous: $k_0 < k_{\perp 1}, k_{\perp 2} < p_\perp$

Figure 7: Schematic graph for a hard $\gamma\gamma$ process, showing the three different scales. To the right is shown the relation to the six classes in the text.

possible transverse/longitudinal combinations. Some examples should be enough:

$$\begin{aligned}
\sigma^{\gamma^*\gamma^*}_{\mathrm{VMD}\times\mathrm{GVMD}}(W^2,Q_1^2,Q_2^2) &= \sum_{V_1=\rho^0,\omega,\phi,\mathrm{J}/\psi} \frac{4\pi\alpha_{\mathrm{em}}}{f_{V_1}^2}\,\left[1+r_i(m_{V_1}^2,Q_1^2)\right]\,\left(\frac{m_{V_1}^2}{m_{V_1}^2+Q_1^2}\right)^2 \times \\
&\times \frac{\alpha_{\mathrm{em}}}{2\pi}\sum_{\mathrm{q}} 2\mathrm{e}_{\mathrm{q}}^2 \int_{k_0^2}^{k_1^2}\frac{\mathrm{d}k_\perp^2}{k_\perp^2}\,\left[1+r_i(4k_\perp^2,Q_2^2)\right] \times \\
&\times \left(\frac{4k_\perp^2}{4k_\perp^2+Q_2^2}\right)^2 \frac{k_{V_2(\mathrm{q}\overline{\mathrm{q}})}^2}{k_\perp^2}\,\sigma^{V_1V_2(\mathrm{q}\overline{\mathrm{q}})}(W^2)\,, \qquad (32)\\
\sigma^{\gamma^*\gamma^*}_{\mathrm{VMD}\times\mathrm{dir}}(W^2,Q_1^2,Q_2^2) &= \sum_{V_1=\rho^0,\omega,\phi,\mathrm{J}/\psi} \frac{4\pi\alpha_{\mathrm{em}}}{f_{V_1}^2}\,\left[1+r_i(m_{V_1}^2,Q_1^2)\right]\,\left(\frac{m_{V_1}^2}{m_{V_1}^2+Q_1^2}\right)^2 \times \\
&\times \left(\sigma_{\mathrm{T}}^{V_1\times\mathrm{dir}}(W^2,Q_2^2)+\sigma_{\mathrm{L}}^{V_1\times\mathrm{dir}}(W^2,Q_2^2)\right)\,. \qquad (33)
\end{aligned}$$

To this should be added the new DIS processes that appear for non-vanishing Q^2, when one photon is direct and the other resolved, i.e. VMD or GVMD. For simplicity, first assume that one of the two photons is real, $Q_2^2 = 0$. For large Q_1^2, this DIS contribution can be given a parton-model interpretation,

$$\sigma^{\gamma^*\gamma}_{\mathrm{DIS}\times\mathrm{res}}(Q_1^2) \simeq \frac{4\pi^2\alpha_{\mathrm{em}}}{Q_1^2}\,F_2^\gamma(x,Q_1^2) \simeq \frac{4\pi^2\alpha_{\mathrm{em}}Q^2}{(Q_1^2+m_\rho^2)^2}\sum_{\mathrm{q}} e_{\mathrm{q}}^2\,\left\{xq^\gamma(x,Q_1^2)+x\overline{q}^\gamma(x,Q_1^2)\right\}\,. \qquad (34)$$

Note that this is only the resolved part of $\sigma_{\mathrm{tot}}^{\gamma^*\gamma}$. The direct contribution from $\gamma^*\gamma \to \mathrm{q}\overline{\mathrm{q}}$ comes in addition, but can be neglected in the leading-order definition of F_2^γ. We will therefore use parton distribution parameterizations for the resolved photon, like SaS 1D [11], to define the $\sigma^{\gamma^*\gamma}_{\mathrm{DIS}\times\mathrm{res}}(Q_1^2)$. Then eq. (31) generalizes to

$$\begin{aligned}
\sigma_{\mathrm{tot}}^{\gamma^*\gamma}(W^2,Q_1^2) &= \sigma^{\gamma^*\gamma}_{\mathrm{DIS}\times\mathrm{res}}\,\exp\left(-\frac{\sigma^{\gamma^*\gamma}_{\mathrm{dir}\times\mathrm{res}}}{\sigma^{\gamma^*\gamma}_{\mathrm{DIS}\times\mathrm{res}}}\right)+\sigma^{\gamma^*\gamma}_{\mathrm{dir}\times\mathrm{res}} \\
&\quad +\sigma^{\gamma^*\gamma}_{\mathrm{res}\times\mathrm{dir}}+\sigma^{\gamma^*\gamma}_{\mathrm{dir}\times\mathrm{dir}}+\left(\frac{W^2}{Q_1^2+W^2}\right)^n\,\sigma^{\gamma^*\gamma}_{\mathrm{res}\times\mathrm{res}}\,. \qquad (35)
\end{aligned}$$

The large-x behaviour of a resolved photon does not agree with that of the proton, but for simplicity we will stay with $n = 3$.

The generalization to both photons virtual then gives

$$\begin{aligned}\sigma_{\mathrm{tot}}^{\gamma^*\gamma^*}(W^2, Q_1^2, Q_2^2) &= \sigma_{\mathrm{DIS}\times\mathrm{res}}^{\gamma^*\gamma^*} \exp\left(-\frac{\sigma_{\mathrm{dir}\times\mathrm{res}}^{\gamma^*\gamma^*}}{\sigma_{\mathrm{DIS}\times\mathrm{res}}^{\gamma^*\gamma^*}}\right) + \sigma_{\mathrm{dir}\times\mathrm{res}}^{\gamma^*\gamma^*} \\ &\quad + \sigma_{\mathrm{res}\times\mathrm{DIS}}^{\gamma^*\gamma^*} \exp\left(-\frac{\sigma_{\mathrm{res}\times\mathrm{dir}}^{\gamma^*\gamma^*}}{\sigma_{\mathrm{res}\times\mathrm{DIS}}^{\gamma^*\gamma^*}}\right) + \sigma_{\mathrm{res}\times\mathrm{dir}}^{\gamma^*\gamma^*} \\ &\quad + \sigma_{\mathrm{dir}\times\mathrm{dir}}^{\gamma^*\gamma^*} + \left(\frac{W^2}{Q_1^2 + Q_2^2 + W^2}\right)^n \sigma_{\mathrm{res}\times\mathrm{res}}^{\gamma^*\gamma^*} , \end{aligned} \tag{36}$$

where the choice of damping factor for the last term again is a simple guess for an extension. When $Q_1^2 \gg Q_2^2$ the expression for $\sigma_{\mathrm{tot}}^{\gamma^*\gamma^*}(W^2, Q_1^2, Q_2^2)$ can be related to the structure function of a virtual photon, $F_2^{\gamma^*}(x, Q^2 = Q_1^2, P^2 = Q_2^2)$, where $x = Q_1^2/(Q_1^2 + Q_2^2 + W^2)$.

A comment about the exponential factors suppressing the DIS terms. Properly, each VMD/GVMD state should come with its ratio of direct to DIS cross sections. However, a number of common factors divide out in this ratio: obviously the probability to fluctuate to the state in question, but partly also the form of the parton distributions in the state. Therefore, it is a good approximation to define a common exponential form for all VMD/GVMD state, based on the weighted average, which is equivalent to using the full resolved term in both numerator and denominator.

2.7 Other Model Aspects

In the preceding section we have mainly described the model as differential in W (invariant mass of the γ^*p or $\gamma^*\gamma^*$ system) and the hardest scales involved: $p_\perp$, $k_{\perp i}$ and Q_i^2. The discussion about the different processes has been limited to the parton-level only, but it is necessary to add parton showers, beam remnants, hadronization etc. in order to simulate complete events. The model is implemented in the PYTHIA 6.151 event generator [21], which includes the above and many other aspects, and it will be used in the following for the results presented. Clearly, here we can only give a few typical examples; with the help of the generator it is possible to study any specific experimental conditions and observables.

While based on the formalism outlined above, the complete event simulation also involves some more model-specific assumptions. We here present a few of those, to try to complement the overall picture. Further refinements are possible in many places, and some of the known shortcomings are mentioned.

The extension from pp to γ^*p and $\gamma^*\gamma^*$ collisions requires two new aspects to be introduced in the event simulation structure. One is the need to construct the $\mathrm{e} \to \mathrm{e}\gamma^*$ kinematics, and to let the collision description depend not only on the resulting W but also on the selected Q^2 virtuality scale(s) of the photon(s). This part was described in [6].

The other is the necessity to mix all the different reaction processes. The main classification is here into 4 components for γ^*p — VMD, GVMD, direct and DIS — and 13 for $\gamma^*\gamma^*$ — 4-squared except that there is no DIS process on a direct photon or another DIS photon. Each of these components has a set of allowed subprocesses, e.g. $\gamma^*\mathrm{q} \to \mathrm{qg}$ and $\gamma^*\mathrm{g} \to \mathrm{q}\overline{\mathrm{q}}$ for direct processes. This set is the same for a VMD and a GVMD photon, but the two are distinguished by the different parton distributions and total cross section

parameterizations used. In the Monte Carlo, a choice is first made between the 4/13 components and then, for that component, among the allowed subprocesses, according to maxima estimated at the initialization. Once the kinematics of the event has been fully selected, the ratio of the actual cross section to the assumed one is used to retain the event or to select a new component and subprocess.

The separation of VMD from GVMD requires access to parton distributions where those two components are explicitly made available separately. Effectively this limits the choice to the SaS parameterizations [11], and with the assumed $k_0 \approx 0.5$ GeV to SaS 1D. An almost equivalent formalism could have been constructed in terms of a common resolved class, so that we could have gone from 4/13 to 3/6 categories. While the calculation of partonic processes would have been simplified, aspects related to total cross section processes (elastic, diffractive, low-$p_\perp$, etc.) would not, so we have not yet tried to construct such a complete alternative machinery.

A VMD photon may be classified either as ρ^0, ω, ϕ or J/ψ. The parameterizations of total, elastic, single and double diffractive cross sections for Vp and V_1V_2 collisions of real photons are given in [15]. The respective inelastic non-diffractive cross section is obtained by subtraction, and sets the envelope within which the jet cross section is eikonalized. The events are ultimately classified, either by the hardest interaction that occurs, or as a low-$p_\perp$ event if there are no hard interactions. For virtual photons, both the total, elastic, single and double diffractive cross sections are dampened by the same dipole factors, cf. eq. (24). The jet cross section is obtained by the virtuality-dependent parton distributions, however, so in the eikonalization procedure the mixture between jet and low-$p_\perp$ events is explicitly Q^2-dependent. For technical reasons, currently it is not possible to mix different dipole factors for the different VMD states, so the ρ/ω mass is used throughout, thus giving a too fast dampening of the (rare) J/ψ events.

For the GVMD states, the mass selection is based on the identification $m \simeq 2k_\perp$ and a $k_\perp$ spectrum e.g. as implied by eq. (29). Thus, neglecting the longitudinal-photon factor, one has a mass spectrum like $\mathrm{d}m^2/(m^2+Q^2)^2$ in the range $2k_0 < m < 2p_{\perp\min}(W^2)$. This spectrum begins at 1 GeV, i.e. a bit above m_ρ. Again there is not yet any provision for heavier quarks in the dipole dampening formulae, but the mass of an $\mathrm{s\overline{s}}$ state is shifted by $m_\phi - m_\rho$ and that of an $\mathrm{c\overline{c}}$ by $m_{\mathrm{J}/\psi} - m_\rho$, to ensure that the GVMD spectrum starts above the lowest-lying state. The mass selected above then becomes the final-state mass of an elastically scattered GVMD particle. A diffractively scattered GVMD is assigned an excited mass according to a spectrum stretching from the selected mass and upwards to the kinematical limit, essentially like $\mathrm{d}m^2/m^2$, as described in [15].

An elastic or diffractive GVMD state is in reality no different from a diffractive VMD state of the same mass. A low-mass system is allowed to decay to two hadrons, whereas more massive ones are considered as strings stretched along the event axis, modulo limited transverse-momentum fluctuations. It is assumed that a simple string is stretched between two endpoint quarks half of the time, and a hairpin string arrangement with a gluon pulled back the other half. Clearly this mixture is only a simple first approximation to what is likely to be a more complex structure [22].

The mass of the GVMD state does not enter the description of inelastic non-diffractive events. However, here the $k_\perp \simeq m/2$ does provide a 'primordial $k_\perp$' kick that can be transmitted to the parton of a hard scattering, not only for GVMD×p but also in processes such as DIS×GVMD. The corresponding number ought to be $k_\perp \approx m_\rho/2$ for VMD and $k_\perp \approx m_\mathrm{p}/3 \approx m_\rho/2$ for a proton. However, in hadronic collisions much higher numbers than that are often required to describe data, typically of the order of 1 GeV [23] if a

Gaussian parameterization is used. Thus, an interpretation as a purely nonperturbative motion inside a hadron is difficult to maintain.

Instead a likely culprit is the initial-state shower algorithm. This is set up to cover the region of hard emissions, but may miss out on some of the softer activity, which inherently borders on nonperturbative physics. By default, the shower does not evolve down to scales below $Q_0 = 1$ GeV; if the $k_\perp \simeq m/2$ scale of a GVMD photon is above this the evolution is stopped already at the larger scale. (Whether Q_0 should best be compared with m or $m/2$ is an open issue.) Any shortfall in shower activity around or below this cutoff then has to be compensated by the primordial $k_\perp$ source, which thereby largely loses its original meaning.

It could be argued that, while a VMD photon should have the same primordial $k_\perp$ spectrum as a hadron, a GVMD one should receive its main contribution from the perturbative $k_\perp \simeq m/2$ contribution, i.e. have a shape like $\mathrm{d}k_\perp^2/(k_\perp^2 + Q^2/4)^2$ in the range $k_0 < k_\perp < p_{\perp\min}(W^2)$. However, this has the questionable consequence that a low-mass GVMD state would have a smaller average 'primordial $k_\perp$' than a VMD one. While we have retained such a possibility as an option, our default has instead been to go to the other extreme, where the partons in a GVMD state has a $k_\perp$ given by the vector sum of the perturbative power spectrum and the same nonperturbative Gaussian smearing as for hadrons. Comparisons with data on photon remnant jets should eventually shed more light on the appropriate procedure.

In most processes, initial- and final-state shower activity is routinely added to the lowest-order process, thereby providing an approximation to higher-order QCD corrections. An exception is the DIS process $\gamma^*\mathrm{q} \to \mathrm{q}$, where currently only final-state radiation has been implemented. The technical reason why the initial-state radiation algorithm does not work here is that it is based on a definition of the z of the splitting kernel as being the fraction by which the $\hat{s}$ of the hard subprocess is reduced by an emission, and $\hat{s} = 0$ in the DIS process above. The traditional z interpretation is sensible if one remembers that the complete DIS hard process is $\mathrm{eq} \to \mathrm{eq}$ rather than only $\gamma^*\mathrm{q} \to \mathrm{q}$. However, since we have split off the photon flux, the complete process is not trivially available currently. For small Q^2 values, this is no major problem, since events with activity above this scale belong to the direct event class. Therefore the shower is constrained only to populate the region below Q^2. The problem may become more severe in the high-Q^2 domain, where DIS processes provide the dominant event class and there is a large phase space for shower activity. That is not the region of main interest to us here, however.

The choice of a formalism, with the virtual photon flux separated from the hard processes, is there for two reasons. One is that it makes it possible to set up selection criteria for an event sample, e.g. on W and Q^2 or in terms of scattered electron energies and angles, that are consistent across the different photon components. Another is that many nonperturbative physics aspects, such as VMD total cross sections, best are formulated in such terms.

Also a few other areas are not fully developed. One example is multiple interactions, where only the simpler impact-parameter-independent option can be used [7], at least until one has constructed a model of the spatial distribution of partons in a GVMD state. On the positive side, options are available for several of the other aspects discussed in this article, so that one may study the sensitivity to the assumptions made.

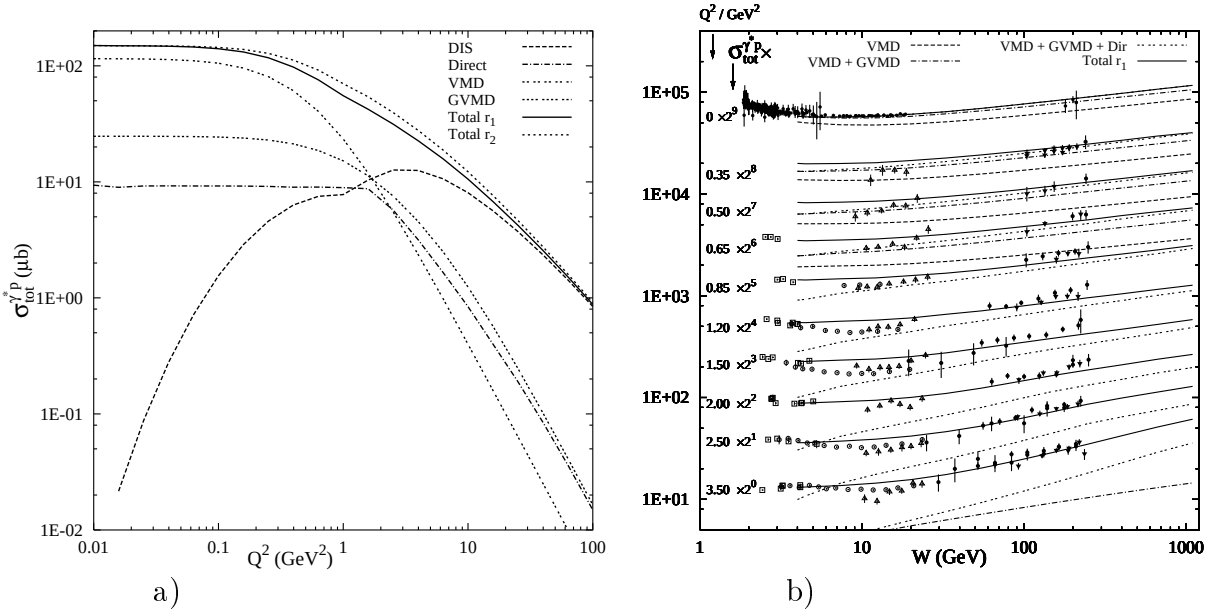

Figure 8: a) The total $\sigma_{\rm tot}^{\gamma^*{\rm p}}$ cross section as function of the photon virtuality at $W_{\gamma^*{\rm p}} = 100$ GeV. The resolved components shown are with alternative r_1 for the longitudinal contribution. b) Contributions to the total $\sigma_{\rm tot}^{\gamma^*{\rm p}}$ cross section from the different event classes: direct, VMD, GVMD and DIS. For simplicity, the VMD and VMD+GVMD contributions are not shown for the lines corresponding to Q^2 values in the range $0.85 - 2.5$ GeV^2. See text for details. The legend for the data points can be found in Fig. 9a.

3 Results

In this section, some examples of event properties will be given, with emphasis on the differences between the direct, VMD and anomalous/GVMD component of the photon. We will concentrate on a few distributions, starting in the photoproduction limit, and then explore how they gradually turn over from being dominated by the resolved processes to finally being dominated by the bare direct and DIS ones as the photon virtuality increases.

Owing to the resolved components of the photon, pp, γp and $\gamma\gamma$ events show similar behaviour for several event properties, such as multiplicity and transverse energy flow. But clearly, differences are expected due to, for example, the additional direct event class in $\gamma\gamma$.

3.1 Total Cross Sections

3.1.1 γ^*p Total Cross Section

The SaS 1D photon parton distribution and the CTEQ5L proton parton distribution will be used throughout in this section if not otherwise stated [11, 24]. In Fig. 8a, the γ^*p cross section at $W_{\gamma^*{\rm p}} = 100$ GeV is shown as a function of the photon virtuality Q^2. The VMD and GVMD components contain contributions from resolved longitudinal photons with the r_1 alternative. An implicit y dependence enters the r_i factors, eq. (26) and (27), to compensate for the difference in photon flux between longitudinally and transversely polarized photons. To estimate the longitudinal contribution to the resolved component in γ^*p cross sections, a fixed y is chosen in order to set the relative amount of transverse

and longitudinal photons. The value of y consequently depends on the beam energy, and at HERA $W_{\gamma^*\mathrm{p}} = 100$ GeV would correspond to $y \simeq 0.1$, a value which will be used in the following. The parameter a, appearing in r_i, is unknown and need to be determined by data. As a starting point for the discussion, a is chosen to 0.5.

In the photoproduction limit, the VMD component dominates the total cross section whereas the DIS one has a vanishing cross section by construction, see Fig. 8a. The GVMD and direct processes share the remaining part, about 20%, of the total cross section. It follows from the introduction of the dipole factors in eq. (24) that, when considering total γ^*p cross sections, the VMD class is the dominating component up to photon virtualities of the order of a vector meson mass. Similarly, the characteristic virtualities for the GVMD class to still be important are of the order of the k_1 parameter discussed in section 2.3.

The direct processes are simulated in the region where the hard scale $k_\perp$ of the photon–parton scattering fulfill $k_\perp > \max(k_1, Q)$, cf. Fig. 5. At low Q^2 values, the $k_1 = p_{\perp\min}(W^2) \simeq 1.3$ GeV provides a fix limit on the available phase space, but at higher Q^2 the phase space shrinks, explaining the kink in Fig. 8a for the direct cross section at $Q^2 = k_1^2$. So it is rather this condition that drives the dampening at large Q^2 than the explicit Q^2 dependence appearing in the matrix elements. A kink can also be seen in the DIS cross section; it is an artifact from the freezing of the parton distributions below their range of applicability (as introduced in section 2.1). Hence, the CTEQ5L proton parton distribution has $Q^2_{\min} = 1$ GeV. The factors introduced for the DIS component, eq. (9), together with the exponential dampening, eq. (23), make the unusual form of the DIS cross section — to be discussed in more detail below.

The proton structure function F_2 has been measured at various x and Q^2 values [25] and is related to the total virtual photon–proton cross section $\sigma_{\mathrm{tot}}^{\gamma^*\mathrm{p}}$ through eq. (7). In Fig. 8b and 9a, $\sigma_{\mathrm{tot}}^{\gamma^*\mathrm{p}}$ is shown from zero Q^2, the total photoproduction cross section [26], to medium Q^2 values as a function of the invariant mass W of the γ^*p-system. Results from the model are compared with data from different fixed-target and HERA experiments. The contribution from the different event classes: direct, VMD, GVMD and DIS are shown in Fig. 8b, and sum up to the total contribution as given in eq. (31). The DIS contribution can be obtained by subtracting the 'VMD+GVMD+Dir' contribution from the 'Total r_1' one. With increasing photon virtuality, the energy dependence of k_1 makes the GVMD states to be less dampened at large energies as compared to low ones. This is also indicated in Fig. 8b by comparing the 'VMD' and 'VMD+GVMD' lines at different Q^2 and W.

In Fig. 9a, the total contribution obtained with different assumptions of the longitudinal contribution for resolved photons are compared to the case with transverse photons only. With the other model assumptions made, a non-vanishing longitudinal contribution is indicated. The alternative with r_1 gives a good fit to data, but overshoots at low W values for some Q^2 values. In the high Q^2 region, showed in Fig. 8a and at the bottom in Fig. 9b, the choice of longitudinal alternative for the resolved component is irrelevant for the total cross section since the resolved event classes give a negligible contribution. Hence, the parameter a should be tuned at intermediate Q^2 values. At lower Q^2 values, however, the r_2 alternative is overshooting data significantly. Taking $a = 0.5$ as a satisfactory value for the r_1 alternative, the r_2 one require $a = 0.2$ to give an equally good description (not shown).

The direct processes increase with $W_{\gamma^*\mathrm{p}}$ faster than the DIS one, and consequently also the exponential suppression of the DIS term. Therefore they contribute substantially

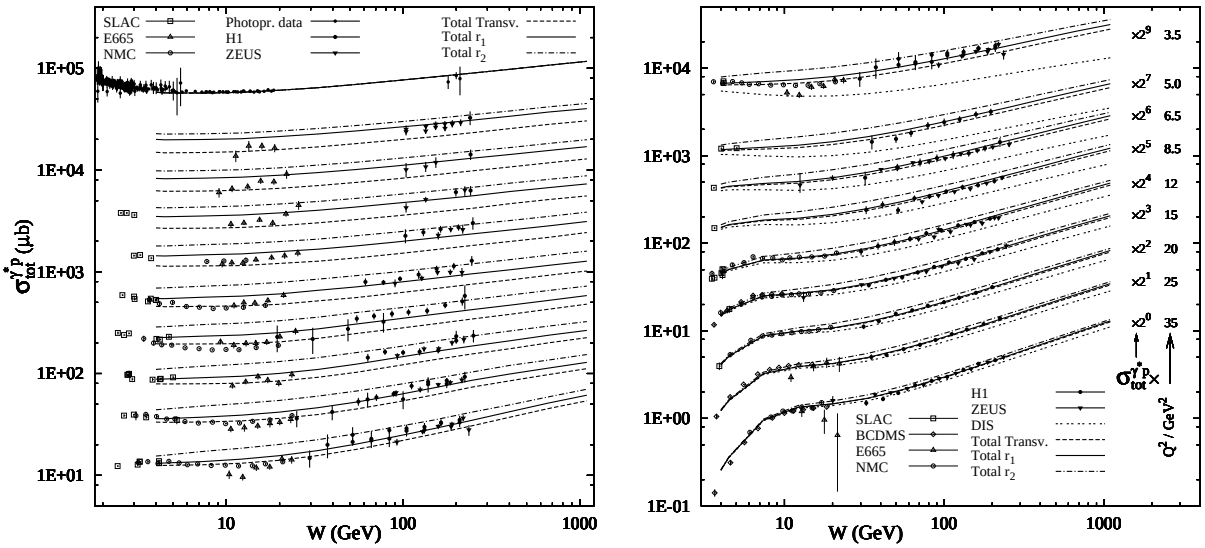

Figure 9: a) The total contribution to $\sigma_{\rm tot}^{\gamma^*{\rm p}}$ from the different event classes. The two different longitudinal alternatives are compared to the case with only transverse photons considered. The data and 'Total r_1' is the same as in Fig. 8b. b) Same as in a but for a different Q^2 range and also the DIS contribution is shown. For reference, the $Q^2 = 3.5$ GeV^2 lines are the same, however.

to the total cross section in the large $W_{\gamma^*{\rm p}}$ (small x) region, even at photon virtualities up to tens of GeV^2, shown for $W_{\gamma^*{\rm p}} = 100$ GeV in Fig. 8a. The DIS and direct classes are often combined and clearly dominate the total cross section at $Q^2 = 3.5$ GeV^2 which is above the m_V^2 and k_1^2 scales of the VMD and GVMD states discussed above. Due to the negligible contribution from the direct processes at $W_{\gamma^*{\rm p}} = 10$ GeV, the exponential suppression factor for the DIS term is close to unity — independently of Q^2. Hence, the sum of the direct and DIS contributions reproduce the $\sigma_{\rm DIS}^{\gamma^*{\rm p}}$ cross section, eq. (22). For $W_{\gamma^*{\rm p}} = 100$ and 1000 GeV this is the case for $Q^2 > 5$ and 8 GeV^2, respectively.

3.1.2 $\gamma^*\gamma$ Total Cross Section

For simplicity, a fixed $y_i = 0.1$ is also used in photon–photon collisions for the calculation of the longitudinal resolved photon contributions. In Fig. 10a, the $\sigma_{\rm tot}^{\gamma^*\gamma}$ at $W_{\gamma^*\gamma} = 100$ GeV is shown as a function of one of the photon virtualities; the other photon is real. The different components are shown separately and sum up to the total contribution with the r_1 alternative. Additionally, relative to the corresponding γ^*p case, the direct cross section enters and starts to be significantly dampened only when $Q_1^2 \simeq W^2$. The kink seen for the single-resolved case can again be explained by the constraint of the hard scale in the scattering process to be larger than the virtuality of the direct photon.

The same distribution is shown for the case of two virtual photons in Fig. 10b. The low virtuality end of Q_1^2 of course corresponds to the cross sections at $Q_1^2 = 10$ GeV^2 in Fig. 10a. The DIS cross section dominates in this region, with the first photon as the target probed by the second one. This is interchanged for $Q_1^2 \geq Q_2^2$. It is noticeable that all the different processes shown are of about the same importance when Q_1^2 is in the neighbourhood of Q_2^2.

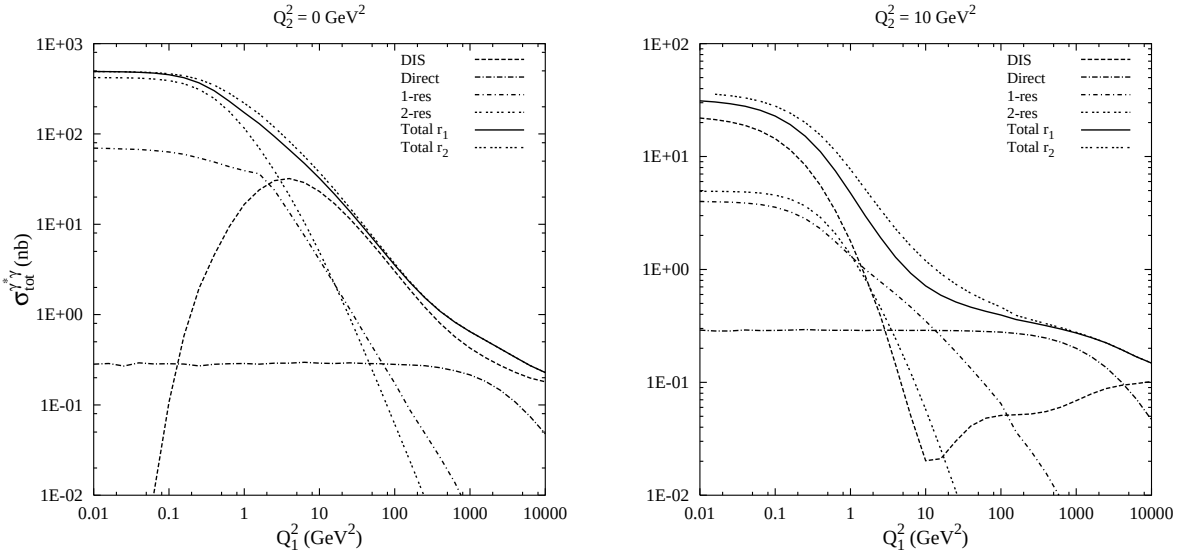

Figure 10: a) The $\sigma_{\rm tot}^{\gamma^*\gamma}$ at $W_{\gamma^*\gamma} = 100$ GeV as a function of the photon virtuality Q_1^2 of one of the photons is shown for the DIS, direct, single-resolved (1-res), double-resolved (2-res) and total contribution. The other photon is real, $Q_2^2 = 0$ GeV^2. b) Same as in a) but for $\gamma^*\gamma^*$ with a target photon virtuality $Q_2^2 = 10$ GeV^2.

For various reasons, the photon F_2^γ measurements [27] are both less precise and available in a smaller kinematical range than in the proton case. In Fig. 11a, the $\sigma_{\rm tot}^{\gamma^*\gamma}$ is shown as a function of W for different Q^2 values, similarly to the study in the previous section. With $a = 0.5$ for both alternatives of the longitudinally resolved photons, data does not discriminate between them. The r_1 alternative is below the high-energy end data points for the $Q^2 = 4.04$ and 5.15 GeV^2 lines but the errors and spread in data do not give an unambiguous conclusion.

Fig. 11b shows the contribution to $\sigma_{\rm tot}^{\gamma^*\gamma}$ for some different event classes at $Q^2 = 9.90$ GeV^2. The direct and DIS ones are dominating at low $\gamma^*\gamma$ invariant masses whereas the single-resolved ones increase in importance at high $W_{\gamma^*\gamma}$. The direct processes show the characteristic $1/W^2$ fall off [6] and thereby give its major contribution to the region where the valence quarks dominate the contribution to F_2^γ. Again, the single-resolved processes (1-res; cf. direct ones in γ^*p) increase with energy, which therefore dampens the DIS term slightly at large $W_{\gamma^*\gamma}$, a region which is dominated by the gluon content of the photon. As resolved processes in γ^*p, double-resolved ones (2-res) in $\gamma^*\gamma$ increase with $W_{\gamma^*\gamma}$.

3.1.3 $\gamma^*\gamma^*$ Total Cross Section

There are hardly any systematic data on $\gamma^*\gamma^*$ cross sections. Prior to the recent and ongoing LEP studies, essentially the only publication is the $F_{\rm eff}$ measurement by PLUTO [28]. A comparison with these data points is found in Fig. 12a. The low W values — the first point is in the resonance region — makes the comparison especially precarious, and the second photon is also not all that virtual with its $\langle Q_2^2 \rangle = 0.35$ GeV^2. The main point of the plot is thus not the acceptable agreement with data, but to illustrate the amount of reduction of the cross section relative to the real-photon alternative $Q_2^2 = 0$ and the

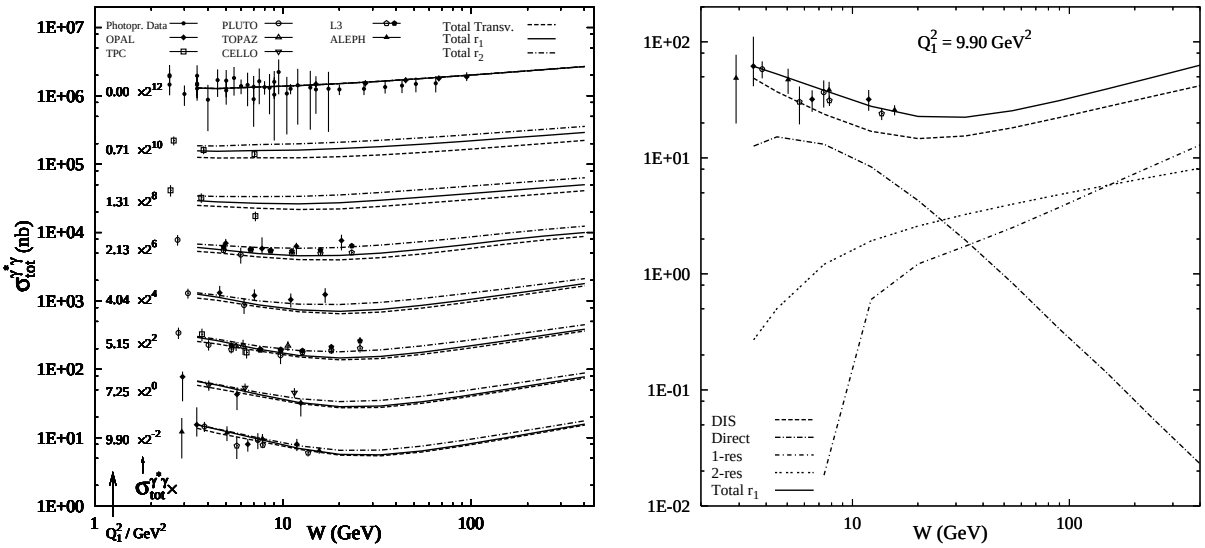

Figure 11: a) Same as in Fig. 9b but for $\gamma^*\gamma$ instead of γ^*p. b) The $\sigma_{\rm tot}^{\gamma^*\gamma}$ as a function of the invariant mass of the $\gamma^*\gamma$ system is shown for the DIS, direct, single-resolved (1-res), double-resolved (2-res) and total contribution.

dependence on assumed longitudinal contributions.

Double-tag two-photon events, $e^+e^- \to e^+e^- +$ hadrons, have been measured by the L3 collaboration [29]. The differential e^+e^- cross section w.r.t. the variable

$$Y = \ln\left(\frac{y_1 y_2 s}{\sqrt{Q_1^2 Q_2^2}}\right) \tag{37}$$

is shown in Fig. 12b. The two scattered leptons are required to be within the polar angle of $30 < \theta_i < 60$ mrad (with respect to the incoming beams) and to have an energy larger than 30 GeV. This plot is expected to provide a clean test of the BFKL behaviour, with a cross section increasing at large Y [30], but the data does not support such a behaviour, or at least less of it than expected. Our model agrees with the data at small Y, but tends to fall below at larger values. This is almost entirely dictated by the drop in the dominant direct contribution. The resolved contributions — which are the ones that could be used to represent a BFKL behaviour in our framework — do come up at large Y, but nowhere near enough to make a significant contribution. We remind that the resolved contributions are suppressed in Q^2 by simple dipole factors; a less steep drop and thereby a larger resolved contribution could be motivated e.g. if the eikonalization of the jet cross section is less significant for a virtual photon. Instead of the conventional increase of the VMD cross section like s^ϵ with $\epsilon \approx 0.08$, eq. (12), a larger effective value like $\epsilon \approx 0.2 - 0.3$ could thus easily be accommodated for virtual photons [31]. For the moment, however, we prefer to await further experimental data. In particular, more detailed analyses of event properties could provide some insight on the relative mixture of event classes at large Y.

3.2 Event Properties

Some event properties are fairly similar between pp, γ^*p and $\gamma^*\gamma^*$, while others differ markedly. The charged multiplicity, Fig. 13, is an example of the former, while the jet

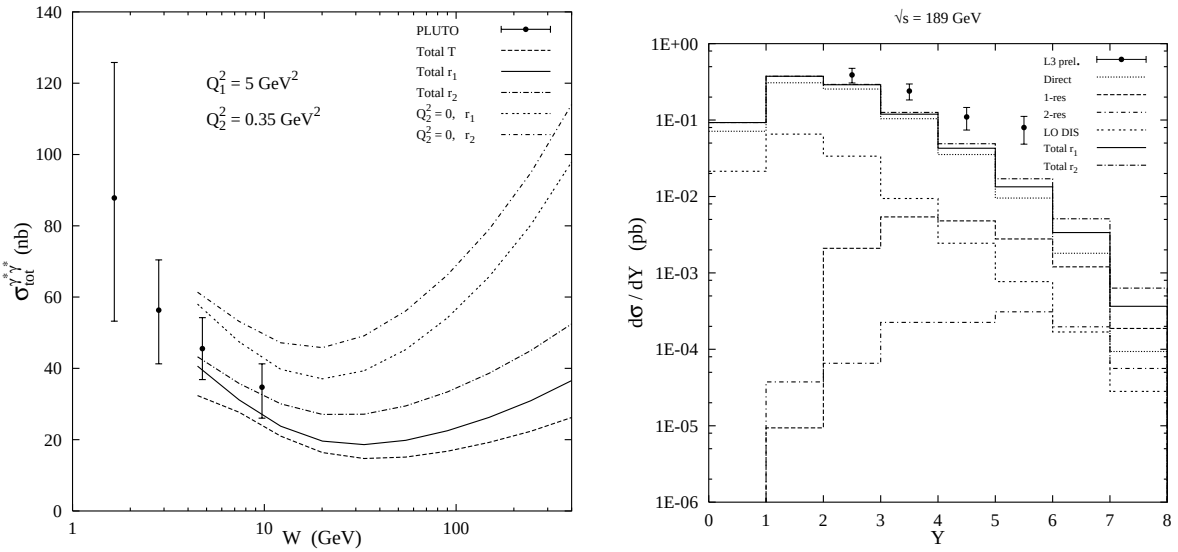

Figure 12: a) The $\sigma_{\rm tot}^{\gamma^*\gamma^*}$ cross section as a function of $W_{\gamma^*\gamma^*}$ for a probing and target photon with virtualities 5 and 0.35 GeV^2 respectively. The data points from PLUTO are obtained from the measured $F_{\rm eff}$ through eq. (7). For reference, the results with a real photon target is shown, $Q_2^2 = 0$ b) The differential $\rm e^+e^- \to e^+e^- + hadrons$ cross section as a function of $Y = \ln(y_1 y_2 s/\sqrt{Q_1^2 Q_2^2})$. The different components shown add up to the 'Total r_1'.

rate, Fig. 14, is of the latter.

Over a wide range of Q^2 values, the γ^*p and $\gamma^*\gamma^*$ events have average charged multiplicities within $\pm 20\%$ of the pp value, Fig. 13a. (Elastic and diffractive events have not been considered. Their inclusion would reduce average multiplicities and change some details, but leave a similar overall picture.) For γ^*p at small Q^2, this is a consequence of the dominance of VMD events, with the characteristic features of hadronic physics, including such aspects as multiple parton–parton interactions. The VMD multiplicity is fairly Q^2-independent, Fig. 13b. The drop to a somewhat lower γ^*p multiplicity around $Q^2 \approx 1 - 10$ GeV^2 instead comes from the transition from VMD dominance to DIS ditto, where the DIS events are cleaner by consisting of only one string piece stretched directly between the kicked-out quark and the beam remnant. Remember that the DIS events here by definition are low-$p_\perp$ ones, with the high-$p_\perp$ part in the direct class, with a higher multiplicity. As the borderline between the two shifts with Q^2, both individually show an increasing multiplicity: the direct by corresponding to a smaller fraction of higher-$p_\perp$ events and the DIS by allowing an increasing admixture of jet events. Figures 13c and 13d show the corresponding Q_1^2 dependence of the $\gamma^*\gamma^*$ multiplicity, for a fixed $Q_2^2 = 1$ GeV^2, normalized to the number of event of each kind and to the total number, respectively. Again the disappearance of the doubly-resolved event class is responsible for a drop in the multiplicity, with the DIS and direct processes taking over. We remind that in $\gamma^*\gamma^*$ the high-$p_\perp$ part of the DIS process is the single-resolved one, corresponding to the direct one of γ^*p, while the $\gamma^*\gamma^*$ direct class has no correspondence in γ^*p.

When it comes to the fraction of events that contain at least one jet, the differences are orders of magnitude, both with a hierarchy of increasing jet fraction from pp to γ^*p to $\gamma^*\gamma^*$, and with an increase as a function of Q^2, Fig. 14a. Again the detailed studies in

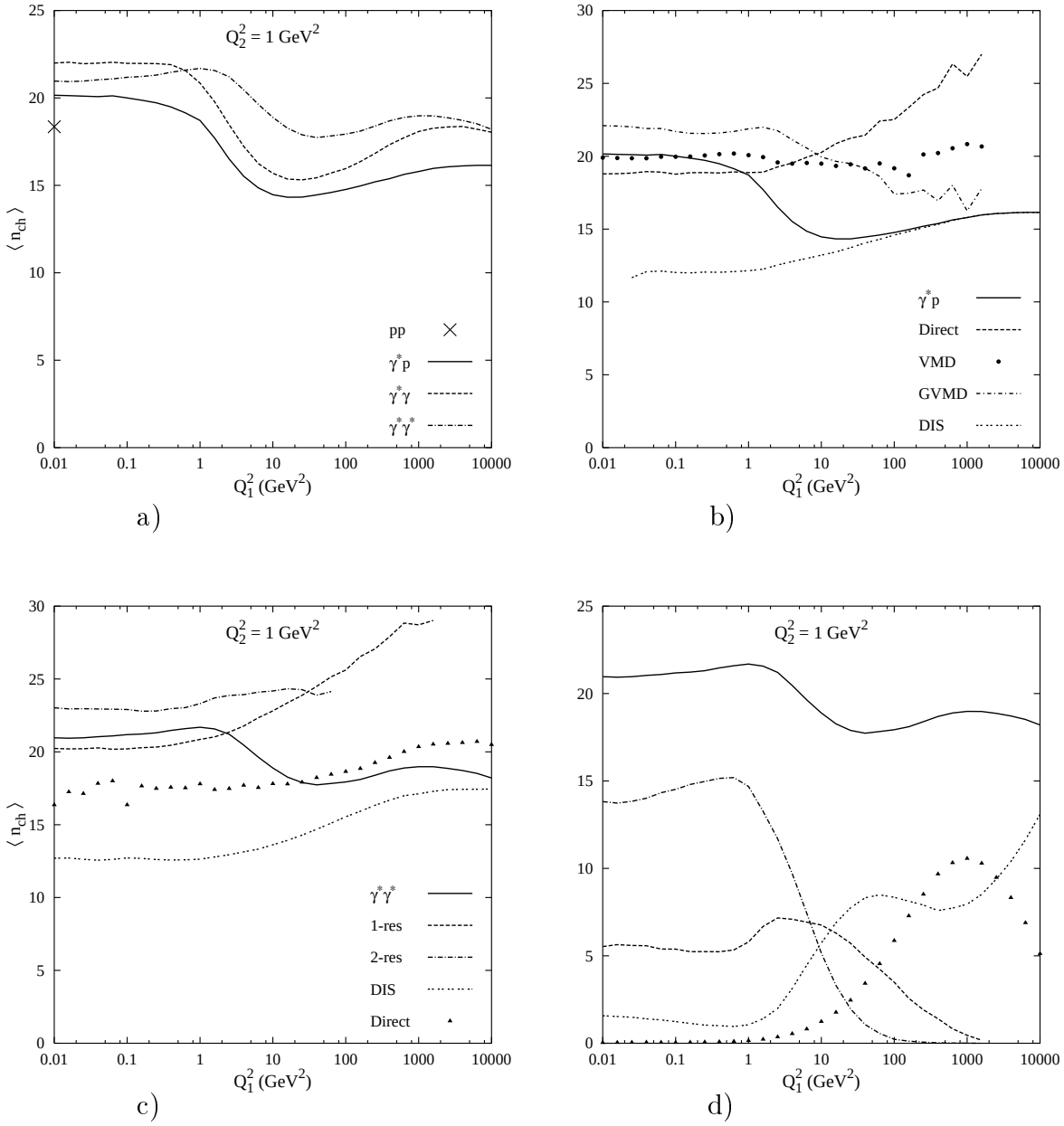

Figure 13: a) The average charged multiplicity $\langle n_{\rm ch} \rangle$ as a function of the photon virtuality for γ^*p, $\gamma^*\gamma$ and $\gamma^*\gamma^*$ events at a center of mass energy of 100 GeV. The result from pp events is indicated with a cross on the y-axis. For the $\gamma^*\gamma^*$ events, the other photon virtuality is kept fixed at $Q_2^2 = 1$ GeV^2. (In $\gamma^*\gamma$ $Q_2^2 = 0$ GeV^2.) No diffractive or elastic events are considered. b) The results from the different components in γ^*p, averaged over the number of events of the respective kind. c) The result from different components in $\gamma^*\gamma^*$, averaged over the number of events of the respective kind. d) As in c) but averaged over the total number of $\gamma^*\gamma^*$ events.

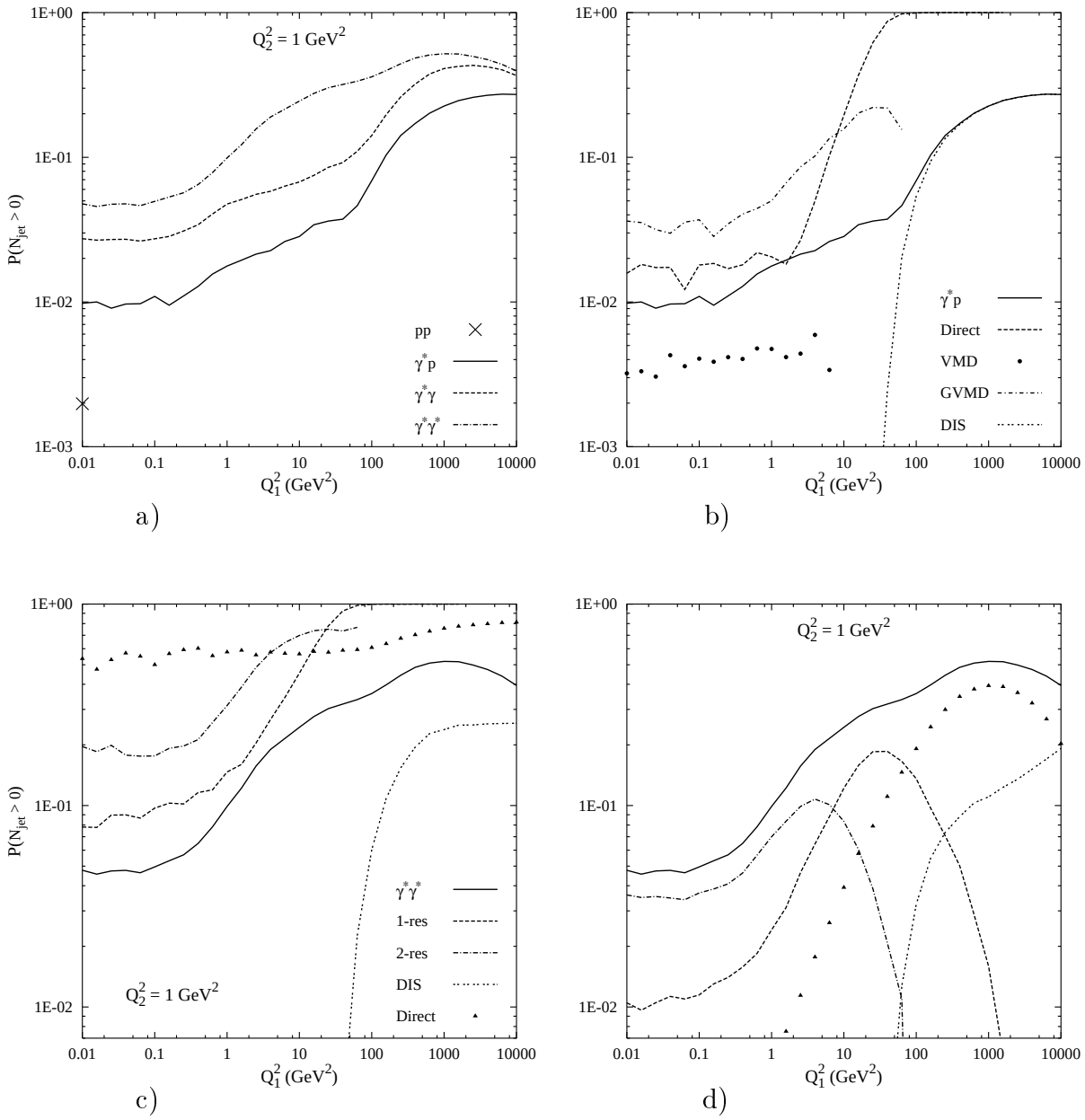

Figure 14: a) The fraction of events that contain at least one jet with an $E_\perp > 5$ GeV inside a cone of radius $R = \sqrt{(\Delta y)^2 + (\Delta\phi)^2} < 1$. $W = 100$ GeV in all cases. No diffractive or elastic events are considered. b) The results from the different components in γ^*p, averaged over the number of events of the respective kind. c) The result from different components in $\gamma^*\gamma^*$, averaged over the number of events of the respective kind. d) As in c) but averaged over the total number of $\gamma^*\gamma^*$ events.

Figs. 14b–d show that the main effect in Q^2 is not in each individual event class but rather in the mixture of the event classes. Thus VMD is similar to pp, with minor differences from parton distributions, while GVMD is higher and direct higher still (at large Q^2). The DIS rate starts vanishing, since events with parton $p_\perp > Q$ are put in the direct class, but eventually comes up for $Q > p_\perp$. In that range, all direct events are required to have jets at lowest order, and only fluctuations in the parton shower and hadronization can occasionally stop jets from being found. For $\gamma^*\gamma^*$ events, shown in Figs. 14c and d, the single- and double-resolved processes show the behaviour of the direct and resolved (VMD plus GVMD) ones, respectively, in γ^*p. The additional direct class increase slowly with Q^2, Fig. 14c, and dominates the jet rate between the single-resolved and DIS dominated regions, peaking at $Q_1^2 = 1000$ GeV^2, Fig. 14d. It is at this point, for this center of mass energy, where the direct matrix elements starts to be suppressed by the large photon virtuality.

The transverse energy flow, as a function of pseudo-rapidity in the center of mass frame of the collision, is shown in Fig. 15. (Again, elastic and diffractive events are not considered.) In Fig. 15a all photons are real except for $\gamma\gamma^*$ where one of them has the virtuality $Q_2^2 = 1$ GeV^2. Here the most interesting aspect is to see how the events differ in the photon and the proton directions, pp being symmetric as well as $\gamma\gamma$ whereas the γp interpolate between the two with the photon in the $\eta > 0$ direction. Comparing the $\gamma\gamma^*$ with the $\gamma\gamma$ case, the single-resolved processes in $\gamma\gamma^*$ has a larger energy flow in the γ^* direction ($\eta < 0$) due to the increased jet activity. On the other hand, for the double-resolved ones it decreases in both hemispheres but less in the γ^* direction. Additionally, the DIS processes come in to play but add on more or less evenly between the two hemispheres at this low virtuality.

In Fig. 15b, the transverse energy flow is shown for three different virtualities in the γ^*p center of mass frame. The major differences again come from the transition of the events from being VMD dominated to being dominated by the DIS processes. This is compensated by an increasing jet activity in the photon direction, giving the rather subtle changes of the total contribution in the photon hemisphere which camouflage the big changes of the relative composition of the different event classes. The different components in γ^*p collisions with $Q_1^2 = 4$ GeV^2 are shown in Fig. 15c, normalized to the number of events of the respective kind. The asymmetry is largest in the direct class, where all of the photon energy goes into the two high-$p_\perp$ jets. The typical $p_\perp$ of the jets is not all that high, however, so at least one of the jets appears at large positive pseudo-rapidities. The VMD and GVMD events are more symmetric, but the virtual photon parton distributions are harder than the corresponding proton one, giving rise to the observed asymmetry. The VMD events are nearly symmetric for the real photon case, whereas for the GVMD ones the asymmetry is still pronounced, as it should be. As expected, the largest contribution in the photon hemisphere is in decreasing order from DIS, direct, GVMD and VMD events, where the direct and GVMD events are of about equal importance.

A slightly asymmetric energy sharing between the two coloured beam remnants in a hadron–hadron kind of collision has been chosen for the results in this section. A more asymmetric energy sharing could also well be imagined, leaving an uncertainty in the model. For example, the energy flow in the VMD events of Fig. 15c could well decrease by several percent for a latter case.

In Fig. 15d, the transverse energy flow for the collision of two photons is shown. One of the photons is kept at $Q_2^2 = 1$ GeV^2 ($\eta < 0$) and the other has $Q_1^2 = 0$, 1 and 4 GeV^2,

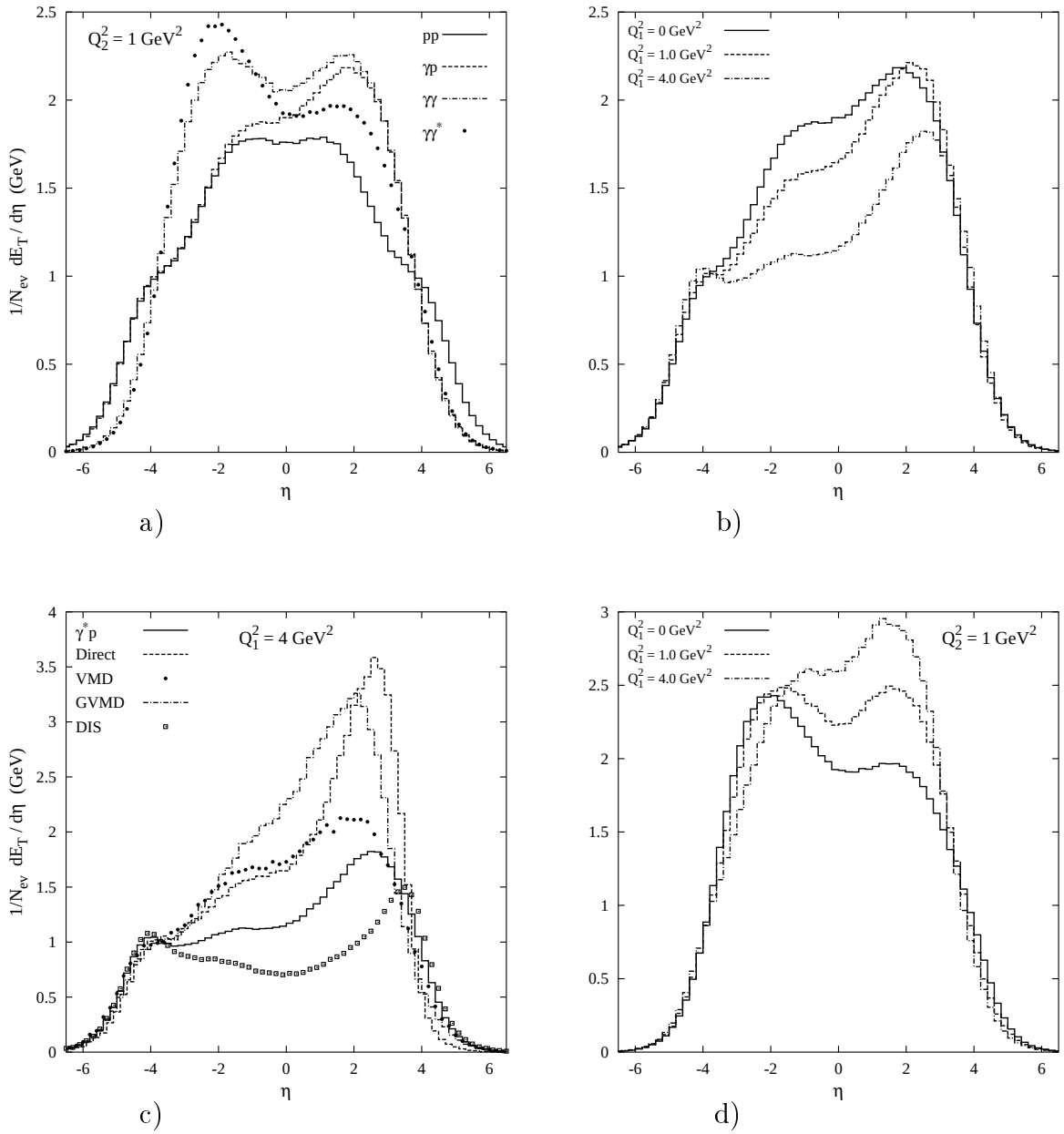

Figure 15: a) The transverse energy flow as a function of pseudo-rapidity in the center of mass frame of the collision, $W = 100$ GeV in all cases. No diffractive or elastic events are considered. b) The transverse energy flow as a function of pseudo-rapidity in the γ^*p center of mass frame, normalized to the number of events. Distributions are shown for photon virtualities of 0, 1.0 and 4.0 GeV^2. c) The different components in γ^*p collisions, normalized to the number of events of the respective kind. The photon virtuality is $Q_1^2 = 4$ GeV^2. d) The transverse energy flow as a function of pseudo-rapidity in the $\gamma^*\gamma^*$ center of mass frame, normalized to the number of events. Distributions are shown for photon virtualities Q_1^2 of 0, 1.0 and 4.0 GeV^2, the other photon has the virtuality $Q_2^2 = 1$ GeV^2.

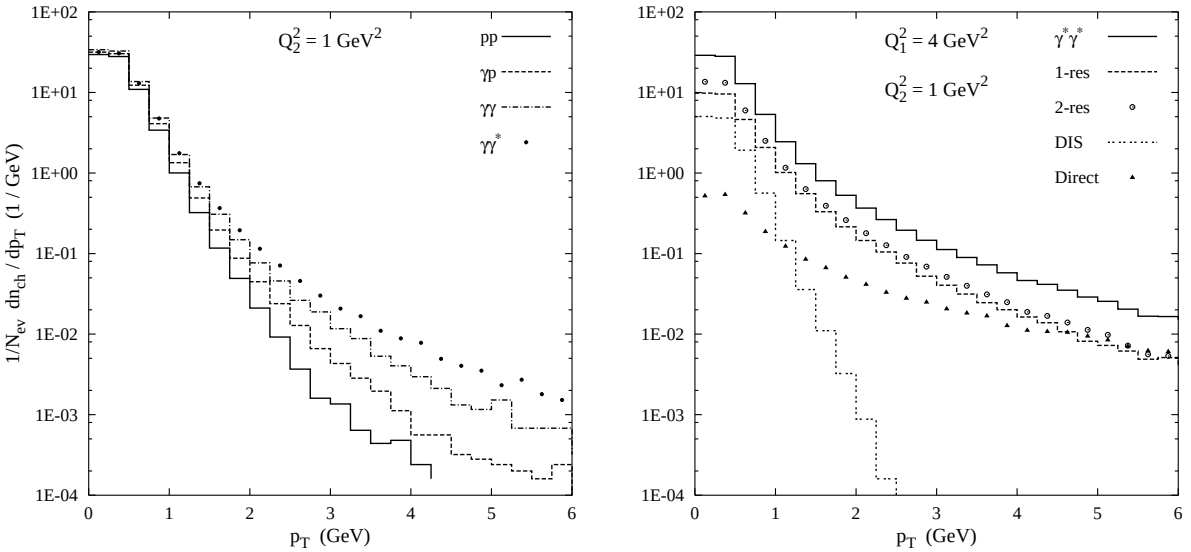

Figure 16: a) The transverse momentum spectra of charged particles for different collisions, normalized to the total number of events. The pseudo–rapidity interval is constrained to [0.5,1.5] (corresponding to the γ direction in case of γp, $\gamma\gamma$ and $\gamma\gamma^*$ collisions). For $\gamma\gamma^*$, one photon is real and the other has a virtuality of $Q_2^2 = 1$ GeV^2. b) With $Q_1^2 = 4$ GeV^2 and $Q_2^2 = 1$ GeV^2, the $\gamma^*\gamma^*$ distribution is shown for the different components; single-resolved, double-resolved, DIS and direct. The sum of them, add up to the full line.

all shown separately. The $Q_1^2 = 0$ GeV^2 distribution was discussed earlier in comparison with two real photons, and is built up by (in order of importance) the asymmetric double- and single-resolved contributions together with a small symmetric DIS contribution — the direct event class is negligible. With both photons having the same virtuality, $Q_i^2 = 1$ GeV^2, the above relative importance between the different components still holds but now all event classes give a symmetric contribution to the $E_\perp$ flow. The last case, with two photons at different virtualities, the single-resolved processes are responsible for most of the asymmetric shape of the total contribution. Now also the direct processes starts to be important with a central plateau of two units in pseudo-rapidity. It is here comparable with the DIS contribution, about 0.25 GeV at central rapidities (normalized to the total number of events).

The transverse momentum spectra of charged particles become harder when going from pp to γp to $\gamma\gamma^*$, Fig. 16, which is partly a reflection of the property of the respective parton distributions and the pattern seen in the jet rates. In γp, the VMD processes dominate in the low end of the spectra and the GVMD and direct processes in the high-$p_\perp$ tail. With increasing photon virtuality, the DIS processes enters but is only of importance at low $p_\perp$ due to the constraint $p_\perp < Q$. (The parton shower and hadronization will cause some particles to be found at $p_\perp > Q$, however.) With a photon virtuality of a few GeV^2, a similar spectra is obtained as for $\gamma^*\gamma^*$ in Fig. 16b, remembering to associate the γp direct events with the $\gamma^*\gamma^*$ single-resolved ones, and the γp resolved with the $\gamma^*\gamma^*$ double-resolved ones.

With two photons, the direct processes give a tail out at high $p_\perp$ that is comparable to the single- and double-resolved processes, Fig. 16b, and contribute to the hardening

of the spectra as compared to pp and γp collisions. When both photons have the same virtuality, for example two real photons, the DIS processes are as usual absent. Although the mixture of event classes differs significantly within a certain kind of collision, the low end of the spectra remain approximately the same when the photon virtuality is increased.

4 Summary and Outlook

We have in this article tried to outline a scenario that covers 'all' photon interactions, whether real or spacelike virtual, that produces hadronic final states. Part of it relies on previous studies, e.g. on jet production with virtual photons or total cross sections for real photons, but here it is eventually combined to give the overall picture. In doing this, we attempt to integrate various aspects into a reasonably consistent overall picture. It would have been nice if a single very economical ansatz for the photon could be made to cover all relevant phenomenology. We do not exclude that this would be possible, although we could also see problems with such an approach. For instance, it appears likely that there really is a fundamental separation into a 'resolved' and a 'direct' (or 'pointlike') part of the photon, e.g. based on the x_γ distributions observed at HERA [32]. Even this separation, of course, is only theoretically well-defined to lowest order, and needs to be prescribed in higher orders of perturbation theory. Nevertheless, the 'all orders' data quite nicely show a separation.

Our model takes such an approach one step further. The resolved part of the photon is subdivided into VMD and GVMD, depending on whether the resolved photon is associated with one of the lowest-lying vector mesons or with one in the set of not so well known higher-mass resonances. For a virtual photon, these states then have a dampened cross section given by dipole form factors. The direct sector is somewhat more complicated, since the lowest-order DIS process $\gamma^*\mathrm{q} \to \mathrm{q}$ is not allowed in the limit $Q^2 \to 0$ while the higher-order direct ones $\gamma^*\mathrm{q} \to \mathrm{qg}$ and $\gamma^*\mathrm{g} \to \mathrm{q\overline{q}}$ are. It therefore requires some care to retain only the latter for $Q^2 = 0$ while equating them with the first-order QCD corrections to the DIS process for large Q^2.

The first test that the mixing makes sense comes from a comparison with the total cross sections of γ^*p and $\gamma^*\gamma^*$ interactions. It is possible to obtain a reasonable description of all the data, although with some disagreement for rather small W, where our language is not expected to survive limited phase-space corrections and exclusive final-state effects anyway. Of course, since we have not even attempted to produce our own sets of parton distributions, but taken existing ones, all the possibilities of tuning are not exhausted by far. Also the inclusion of the effects of longitudinal resolved photons remains an area where little is known, and our simpleminded ansatz could be made more sophisticated, e.g. by the use of parton distributions designed to describe the partonic structure of longitudinal virtual photons [33]. However, the model is so far limited to the SaS 1D set of parton distributions. An alternative approach with a common resolved class could have been taken, facilitating the handling of the partonic processes, but probably ending up with a more complicated picture for other aspects such as elastic and diffractive scattering, multiple parton–parton interactions, etc. and at the same time losing the flexibility of having the non-perturbative part of the photon structure separated from the perturbatively calculable one. It is a subject for further studies, however.

More sophisticated tests come from the study of event shapes. We have in this article provided some examples how event properties vary between different initial states and

photon virtualities. The examples are mainly chosen as simple illustrations; we look forward to more detailed studies by the experimental community, based on the code we now provide in the PYTHIA event generator. Again one cannot expect perfect agreement, but at least an overall such, where disagreements hopefully could help provide hints in which direction to move for an even better and more complete picture. In this sense, our model could be seen as a straw man, although a rather more sophisticated such than is often the case.

Given the fairly complex description, we do not expect the model to be competitive in the high-Q^2 region of HERA, say for $Q^2 > 10$ GeV^2. There the simple DIS language provides a powerful starting point, that has been well studied over the years, with many models developed in extensive detail [34]. We are here more interested in the crossover region, $Q^2 \sim 0.5 - 5$ GeV^2, where our model predicts all of the photon components to have comparable cross sections, and we therefore would expect no simple picture to work. In $\gamma^*\gamma^*$ studies at LEP2, it is enough to have one photon in this region for our approach to offer interesting alternatives to other descriptions [35]. For smaller Q^2, it smoothly attaches to the existing PYTHIA model of real-photon interactions, while the high-Q^2 end has no such correspondence.

There are some areas where we already now know that not enough effort has gone in to cover the field. One such is the treatment of heavy flavours and in particular charm production, both open and closed (primarily J/ψ), where mass effects are very important. For the lighter quarks, like the u one, the intrinsic 'current algebra' mass is negligible relative to the 'constituent' one, that sets the scale e.g. of the ρ mass. But for a complete charm description, both the impact of the current algebra mass scale and of the further QCD-induced confinement mass effects have to be considered. Another example of a missing area is that related to rapidity gaps, which are already included in the VMD/GVMD sector within a traditional Regge language, but currently not in the DIS region, in spite of the quite conclusive evidence for this from HERA [36]. The two aspects come together in the W dependence of the production rate of exclusive vector mesons, where data show a steeper rise for J/ψ than lighter mesons, and a steeper rise also at larger Q^2 [31]. On the technical side, initial-state radiation remains to be implemented for the lower-$p_\perp$ DIS process (but is there in the higher-$p_\perp$ direct ones).

Therefore the current model should not be considered as the end of the road, but rather as providing a basic framework that could be further refined. In the end, data will have to tell whether the approach as such is viable or not. In the latter case, a simpler scenario would then be preferable, but more likely an even more complex one would be required.

References

[1] E. Mirkes and D. Zeppenfeld, *Phys. Lett.* **B380** (1996) 105;
S. Frixione and G. Ridolfi, *Nucl. Phys.* **B507** (1997) 315;
M. Klasen, T. Kleinwort and G. Kramer, *Eur. Phys. J.* **C1** (1998) 1;
B.W. Harris and J.F. Owens, *Phys. Rev.* **D57** (1998) 5555;
P. Aurenche, L. Bourhis, M. Fontannaz, J.Ph. Guillet, hep-ph/0006011.

[2] V.N. Gribov and L.N. Lipatov, *Sov. J. Nucl. Phys.* **15** (1972) 438 and 675;
G. Altarelli and G. Parisi, *Nucl. Phys.* **B126** (1977) 298;
Yu.L. Dokshitzer, *Sov. Phys. JETP* **46** (1977) 641.

[3] M. Ciafaloni, *Nucl. Phys.* **B296** (1988) 49;
S. Catani, F. Fiorani and G. Marchesini, *Phys. Lett.* **B234** (1990) 339,
Nucl. Phys. **B336** (1990) 18.

[4] B. Andersson, G. Gustafson and J. Samuelsson, *Nucl. Phys.* **B467** (1996) 443;
B. Andersson, G. Gustafson and H. Kharraziha, *Phys. Rev.* **D57** (1998) 5543;
H. Kharraziha and L. Lönnblad, *J. High Energy Phys.* **03** (1998) 006.

[5] A. Levy and U. Maor, *Phys. Lett.* **B182** (1986) 108;
H. Abramowicz et al., *Phys. Lett.* **B269** (1991) 465;
B. Badelek and J. Kwiecinski, *Phys. Lett.* **B295** (1992) 263;
A. Donnachie and P.V. Landshoff, *Phys. Lett.* **B437** (1998) 408.

[6] C. Friberg and T. Sjöstrand, *Eur. Phys. J.* **C13** (2000) 151 (hep-ph/9907245),
and references therein.

[7] T. Sjöstrand and M. van Zijl, *Phys. Rev.* **D36** (1987) 2019.

[8] L. N. Hand, *Phys. Rev.* **129** (1963) 1834.

[9] V. M. Budnev, I. F. Ginzburg, G. V. Meledin and V. G. Serbo,
Phys. Rept. **15** (1974) 181.

[10] T. H. Bauer et al., *Rev. Mod. Phys.* **50** (1978) 261.

[11] G.A. Schuler and T. Sjöstrand, *Z. Phys.* **C68** (1995) 607,
Phys. Lett. **B376** (1996) 193.

[12] G.A. Schuler and T. Sjöstrand, *Phys. Lett.* **B300** (1993) 169,
Nucl. Phys. **B407** (1993) 539.

[13] A. Donnachie and P.V. Landshoff, *Phys. Lett.* **B296** (1992) 227.

[14] J. Dischler and T. Sjöstrand, in preparation.

[15] G.A. Schuler and T. Sjöstrand, *Z. Phys.* **C73** (1997) 677.

[16] T. Sjöstrand, in 'Multiparticle Dynamics 1994', eds. A. Giovannini et al.
(World Scientific, Singapore, 1995), p. 221.

[17] I.I. Balitsky and L.N. Lipatov, *Sov. J. Nucl. Phys.* **28** (1978) 822,
Yad. Fiz. **28** (1978) 1597;
E.A. Kuraev, L.N. Lipatov and V.S. Fadin, *Sov. Phys. JETP* **45** (1977) 199,
Zh. Eksp. Teor. Fiz. **72** (1977) 377.

[18] H. Fraas and D. Schildknecht, *Nucl. Phys.* **B14** (1969) 543.

[19] BCDMS Collaboration, A.C. Benvenuti et al., *Phys. Lett.* **B223** (1989) 485;
H1 Collaboration, C. Adloff et al., *Phys. Lett.* **B393** (1997) 452;
HERMES Collaboration, K. Ackerstaff et al., *Phys. Lett.* **B475** (2000) 386.

[20] J. J. Sakurai, *Phys. Rev. Lett.* **22** (1969) 981.

[21] T. Sjöstrand, *Computer Phys. Commun.* **82** (1994) 74;
http://www.thep.lu.se/∼torbjorn/Pythia.html.

[22] G. Ingelman and P.E. Schlein, *Phys. Lett.* **152B** (1985) 256.

[23] EMC Collaboration, M. Arneodo et al., *Z. Phys.* **C36** (1987) 527;
L. Apanasevich et al., *Phys. Rev.* **D59** (1999) 074007;
G. Miu and T. Sjöstrand, *Phys. Lett.* **B449** (1999) 313;
C. Bálazs, J. Huston and I. Puljak, hep-ph/0002032.

[24] CTEQ Collaboration, H. L. Lai et al., *Eur. Phys. J.* **C12** (2000) 375.

[25] T. Gehrmann, R.G. Roberts and M.R. Whalley, *J. Phys.* **G25** (1999) A1;
BCDMS Collaboration, A.C. Benvenuti et al., *Phys. Lett.* **223B** (1989) 485;
SLAC Collaboration, L.W. Whitlow et al., *Phys. Lett.* **B282** (1992) 475;
E665 Collaboration, M.R. Adams et al., *Phys. Rev.* **D54** (1996) 3006;
NMC Collaboration, M. Arneodo et al., *Nucl. Phys.* **B483** (1997) 3;
H1 Collaboration, S. Aid et al., *Nucl. Phys.* **B470** (1996) 3, C. Adloff et al.,
Nucl. Phys. **B497** (1996) 3;
ZEUS Collaboration, M. Derrick et al., *Z. Phys.* **C72** (1996) 399, J. Brietweg et al.,
Phys. Lett. **B407** (1997) 432, *Eur. Phys. J.* **C7** (1999) 609.

[26] Particle Data Group, C. Caso et al., *Eur. Phys. J.* **C3** (1998) 1;
ZEUS Collaboration, M. Derrick et al., *Phys. Lett.* **293B** (1992) 465,
Z. Phys. **C63** (1994) 391;
H1 Collaboration, S. Aid et al., *Z. Phys.* **C69** (1995) 27.

[27] TPC/2γ Collaboration, H. Aihara et al., *Z. Phys.* **C34** (1987) 1,
Phys. Rev. Lett. **58** (1997) 97;
PLUTO Collaboration, Ch. Berger et al., *Z. Phys.* **C26** (1984) 353,
Nucl. Phys. **B281** (1987) 365;
CELLO Collaboration, H.J. Behrend et al., contributed paper to the XXVth Int.
Conf. on HEP, Singapore, 1990;
TOPAZ Collaboration, K. Muramatsu et al., *Phys. Lett.* **B332** (1994) 477;
OPAL Collaboration, K. Ackerstaff et al., *Z. Phys.* **C74** (1997) 33,
Phys. Lett. **B411** (1997) 387, *Phys. Lett.* **B412** (1997) 225, G. Abbiendi et al.,
Eur. Phys. J. **C14** (2000) 199;
L3 Collaboration, M. Acciarri et al., *Phys. Lett.* **B436** (1998) 403,
Phys. Lett. **B447** (1999) 147;
ALEPH Collaboration, R. Barate et al., *Phys. Lett.* **B458** (1999) 152.

[28] PLUTO Collaboration, Ch. Berger et al., *Phys. Lett.* **B142** (1984) 119.

[29] L3 Collaboration, M. Acciarri et al., *Phys. Lett.* **B453** (1999) 333.

[30] J. Bartels, A. De Roeck and H. Lotter, *Phys. Lett.* **B389** (1996) 742;
S.J. Brodsky, F. Hautmann and D.E. Soper, *Phys. Rev.* **D56** (1997) 6957.

[31] B. Waugh, *Nucl. Phys.* **B82** *(Proc. Suppl.)* (2000) 262, and references therein.

[32] ZEUS Collaboration, M. Derrick et al., *Phys. Lett.* **B322** (1994) 287;
H1 Collaboration, T. Ahmed et al., *Nucl. Phys.* **B445** (1995) 195.

[33] J. Chýla, PRA-HEP 00-03 (hep-ph/0006232).

[34] 'Monte Carlo Generators for HERA Physics', eds. A.T. Doyle, G. Grindhammer, G. Ingelman and H. Jung, DESY-PROC-1999-02.

[35] L. Lönnblad, M. Seymour et al., in 'Physics at LEP2', eds. G. Altarelli, T. Sjöstrand and F. Zwirner, CERN 96-01, Vol. 2, p. 187;
T. Alderweireld et al., 'Event generators for gamma-gamma physics', to appear in the Proceedings of the LEP2 Monte Carlo Workshop.

[36] ZEUS Collaboration, M. Derrick et al., *Phys. Lett.* **B315** (1993) 481;
H1 Collaboration, T. Ahmed et al., *Nucl. Phys.* **B429** (1994) 477.